Integrated Single-Cell Multiomic Profiling of Caudate Nucleus Suggests Key Mechanisms in Alcohol Use Disorder

Nick Green[1], Hongyu Gao[1,2], Xiaona Chu[1], Quiyue Yuan[3], Patrick McGuire[1], Dongbing Lai[1], Guanglong Jiang[1], Xiaoling Xuei[1], Jill Reiter[1], Julia Stevens[4], Greg Sutherland[4], Alison Goate[5, 6], Zhiping Pang[7,8], Paul Slesinger[5], Ronald P. Hart[7,9], Jay A. Tischfield[10], Arpana Agrawal[11], Yue Wang[1], Zhana Duren[3], Howard J. Edenberg[1,12], Yunlong Liu[1,2]

[1] Indiana University School of Medicine, Department of Medical and Molecular Genetics, Indianapolis, Indiana, 46202, United States
[2] Center for Computational Biology and Bioinformatics, Indiana University School of Medicine, Indianapolis, Indiana, 46202, United States
[3] Clemson University, Department of Genetics and Biochemistry, Greenwood, SC 29646, United States
[4] New South Wales Brain Tissue Research Centre, Charles Perkins Centre and School of Medical Sciences, Faculty of Medicine and Health, The University of Sydney, Camperdown, NSW 2006, Australia
[5] Nash Family Department of Neuroscience, Icahn School of Medicine at Mount Sinai, New York, New York 10029, United States
[6] Department of Genetics & Genomic Sciences, Icahn School of Medicine at Mount Sinai, New York, New York 10029, United States
[7] Human Genetics Institute, Rutgers University, Piscataway, New Jersey 08854, United States
[8] Department of Neuroscience and Cell Biology and The Child Health Institute of New Jersey, Rutgers Robert Wood Johnson Medical School, New Brunswick, New Jersey 08901, United States
[9] Department of Cell Biology & Neuroscience, Rutgers University, Piscataway, New Jersey 08854, United States
[10] Department of Genetics, Rutgers University, Piscataway, New Jersey, United States
[11] Department of Psychiatry, Washington University School of Medicine in St. Louis, St. Louis, Missouri, United States
[12] Department of Biochemistry and Molecular Biology, Indiana University School of Medicine, Indianapolis, Indiana 46202, United States

Abstract

Alcohol use disorder (AUD) is likely associated with complex transcriptional alterations in addiction-relevant brain regions. We characterize AUD-associated differences in cell type-specific gene expression and chromatin accessibility in the caudate nucleus by conducting a single-nucleus RNA-seq assay and a single-nucleus RNA-seq + ATAC-seq (multiome) assay on caudate tissue from 143 human postmortem brains (74 with AUD). We identified 17 cell types. AUD was associated with a higher proportion of microglia in an activated state and more astrocytes in a reactive state. There was widespread evidence for differentially expressed genes across cell types with the most identified in oligodendrocytes and astrocytes, including genes involved in immune

response and synaptic regulation, many of which appeared to be regulated in part by *JUND* and *OLIG2*. Microglia-astrocyte communication via interleukin-1 beta, and microglia-astrocyte-oligodendrocyte interaction via transforming growth factor beta 1 were increased in individuals with AUD. Expression quantitative trait loci analysis revealed potential driver genes of AUD, including *ADAL,* that may protect against AUD in medium spiny neurons and interneurons. This work provides a thorough profile of the effects of AUD in the human brain and identifies several promising genes for further study.

Introduction

Excessive alcohol use creates many serious physical, emotional, and social problems and is responsible for about 3 million deaths worldwide each year.[1] Many alcohol-attributable deaths in the United States result from alcohol use disorder (AUD) (nccd.cdc.gov/DPH_ARDI). AUD is a serious and common psychiatric disorder that is characterized by excessive alcohol consumption and consequent physiological features, alongside psychological and interpersonal problems stemming from preoccupation with and a loss of control over drinking.[2] In addition to excessive alcohol consumption, the risk of developing alcohol use disorder (AUD) depends on both genetic and environmental factors. While recent large-scale genome-wide association studies (GWAS) have identified hundreds of variants associated with alcohol consumption[3,4] and AUD[5-7], it is not yet clear how these variants contribute to AUD.

Beyond these predisposing differences in the static genome, AUD is likely associated with dynamic alterations in gene expression and chromatin conformation, plausibly in brain regions associated with onset and maintenance of motivated and rewarding behaviors, stress responsivity and cognitive control. The consumption of alcohol, or chronic exposure to ethanol modifies gene expression. An early study using microarray analysis to study the effects of chronic ethanol consumption in the nucleus accumbens of rats found significant changes in expression in many genes[8]. Subsequent bulk RNA-sequencing (RNA-seq) studies have uncovered differentially expressed genes in several brain regions, including the hippocampus,[9] prefrontal cortex[10,11], and the striatum[12].

However, the individual brain regions represent a diversity of cell types that may bear unique transcriptional signatures. These cell-specific patterns cannot be identified in bulk RNA sequencing data, even with computational deconvolution techniques. Single-cell/single-nucleus RNA sequencing has enabled measurement of the distribution and characterization of different cell types in a tissue sample and of gene expression in each of these individual cells. An early single-nucleus RNA sequencing (snRNA-seq) study examined gene expression in nuclei from the prefrontal cortex of individuals with and without AUD.[13] Despite a small sample size (7 individuals), they identified seven major cortical cell types, and found differences in expression associated with AUD within six

cell types, notably in astrocytes, oligodendrocytes and microglia, including in neuroinflammation-related genes.

Changes in gene expression may have manifold etiologies. One likely epigenetic precursor is the extent of accessible chromatin that exerts a *cis*-regulatory effect on gene expression. For example, a recent study, using an assay for transposase-accessible chromatin with sequencing (ATAC-seq[14]), identified differences in chromatin accessibility associated with chronic and acute alcohol exposure in the rat amygdala[15]. However, AUD-associated linkages between open chromatin regions and gene expression may be regionally and cell-type specific. The advent of single nucleus multiome experiments, that is, co-assaying both chromatin accessibility and gene expression within the same cell, provides remarkable opportunities to draw causal inferences regarding mechanisms underlying AUD-associated gene expression.

Along with the putamen, the caudate nucleus comprises the dorsal striatum (and more broadly, the basal ganglia), a key component of the executive control loop that is recruited in the onset and maintenance of AUD.[16] The caudate has been implicated in cue-elicited activation, dopamine increase, and in subjective reports of craving.[17,18] In animal models, chronic ethanol exposure alters neural circuits in the basal ganglia[19,20] with a recent study reporting differences in gene expression in the dorsal striatum of alcohol-preferring rats[21]. A transcription-wide association study found that, among 13 human brain tissues, the caudate was the region with the most genes whose predicted expression was associated with problematic alcohol use, a trait that combines AUD with problematic alcohol drinking[5]. However, the caudate harbors multiple cell-types[22] and cell-type-specific characterization of the AUD-associated transcriptome in the human caudate is lacking.

To meet this gap in knowledge, we sought to provide a comprehensive view of AUD-related gene expression and chromatin accessibility differences in specific cell types within in the human caudate nucleus and infer mechanisms underlying these changes. Here, we performed a high-throughput snRNA-seq experiment on human postmortem samples from the caudate nucleus of 143 donors, 74 with and 69 without AUD. We obtained transcriptomic data from over 1.1 million cells. To compare the transcriptome with the open chromatin status of the same cells, we also performed a sn-multiome experiment on samples from these same brains. This dual-experiment approach allowed us to both robustly identify rare cell types and measure small differences in gene expression while also providing a measure of both gene expression and chromatin accessibility in the same nuclei. We identified AUD-associated differences in gene expression and chromatin accessibility in different cell types, the biological pathways underlying these differences, and AUD-associated differences in transcription factor activity and cell-cell communication in major glial cell types (Fig. 1). This study provides a comprehensive profile of AUD-related differences in the caudate nucleus and identifies potential mechanisms of AUD and novel directions for further exploration.

Results

Characterization of 17 Major Cell Types in the Caudate Nucleus

Samples from the caudate nucleus of post-mortem brains from the New South Wales Brain Tissue Resource Centre at the University of Sydney were sequenced in the sn-Multiome assay using a 10X Chromium system, in which transcription levels and chromatin accessibility were measured in the same nuclei, and most also sequenced in the 10X HT snRNA-seq assay. After demultiplexing and data processing, samples with < 200 cell barcodes were removed, leaving 163 samples – 82 with and 81 without AUD; 128 male and 34 female. Low quality nuclei were identified – based on number of genes, number of molecules, and percentage of mitochondrial DNA (see 'Initial Quality Control' in Online Methods) – and removed from all further analyses, leaving gene expression levels for 1,307,323 nuclei and chromatin accessibility (ATAC-seq) for 267,100 of these nuclei (Demographics are in Supplementary Tables 1-2, and detailed experimental procedures are in Online Methods). Graph-based clustering of the snRNA-seq data of the 163 samples identified 17 distinct cell clusters (Fig. 2A, B). Three subtypes of medium spiny neurons (MSNs, the GABAergic projection neurons of the striatum) were identified: D1-type MSNs, D2-type MSNs, and a third subtype marked by both *DRD1* and *DRD2* expression (D1/D2 neurons). Four populations of GABAergic interneurons were identified, including parvalbumin-expressing fast-spiking (FS), neuropeptide Y/somatostatin/nitric oxide synthase-expressing low threshold-spiking (LTS), calretinin-expressing (CR), and cholecystokinin-expressing (CCK). A small cluster of cholinergic neurons was also identified (Ach). In addition to neurons, several glial cell populations were observed, including oligodendrocytes (the most prevalent cell type; 28.2% of the nuclei), oligodendrocyte progenitor cells (OPCs), astrocytes, ependymal cells, and microglia. Other cell types identified include non-microglial macrophages, endothelial cells, and vascular smooth muscle cells.

Glutamatergic neurons were also found; but because the caudate is known not to contain cell bodies of excitatory neurons, their presence might be due to inclusion of parts of another region. Therefore, twenty samples that contained >10% of glutamatergic neurons were removed from all subsequent analyses (Supplementary Tables 1, 2), leaving 143 samples (74 with AUD, 69 without; 115 male, 28 female) with gene expression data for 1,121,762 nuclei, 250,537 of which also had ATAC data. There was no significant difference in relative abundance of cell types between samples from individuals with AUD and those without (Extended Data Figure 1).

Graph-based subclustering was performed for several cell types separately, using cells from the 143 samples. There were four subclusters of microglia, which roughly correspond to different states of microglial activation (Fig. 2C, Extended Data Fig. 2, Supplementary Tables 3-4). Subcluster 1 ("Resting Microglia") uniquely expressed genes specific to quiescent microglia, such as *P2RY12* and *CX3CR1,* and was enriched for pathways relating to microglia migration. Subclusters 2 and 3 were both enriched for immune response-related genes, with subcluster 2 ("Inflammatory Microglia") highly

expressing genes involved in inflammation, such as *TLR2*. Subcluster 3 (CD83+ Microglia) was enriched for genes governing microglia activation, such as *CD83*[23]. Subcluster 4 ("Phagocytosing Microglia") was marked by high expression of genes involved in endocytosis and phagocytosis. There was a significant increase in the mean proportion of "Inflammatory Microglia" (subcluster 2) in individuals with AUD: 31%, as opposed to 23% in control samples (*padj* = 0.027). Individuals with over 50% of microglia cells in the inflammatory state predominantly had AUD (70%, compared to 52%) (Fig. 2D). There was a significant increase with age in the mean proportion of microglia in the inflammatory state in individuals with AUD (p = 0.029).

A larger astrocyte subcluster ("Synaptic Astrocytes") was marked by higher expression of excitatory amino acid transporters 1 and 2 (both glutamate transporters), glutamate receptor 2 (an AMPA receptor subunit), and glutamate synthase, suggesting that these astrocytes may play a role in maintaining glutamatergic synapses (Fig. 2E, Supplementary Tables 5-6). The other subcluster ("Structural Astrocytes") was marked by higher expression of cytoskeleton-related protein-coding genes *GFAP* and *DCLK1*, extracellular matrix protein tenascin C, as well as *CD44*, coding for a protein involved in cell adhesion and migration, and might be more involved in structural support or tissue repair.

Finally, there were two subclusters of both D1 and D2-type neurons, representing matrix and striosome compartments,[24] based on expression of genes specific to either the matrix or striosome regions of the striatum[25] (Extended Data Fig. 2-3). 80% of D1 neurons and 83% of D2 neurons were within the matrix compartment, which makes up approximately 85% of the striatum.[24] There was not a significant difference in subcluster proportion by AUD status in either astrocytes or D1 and D2-type neurons.

AUD-Associated Differences in Gene Expression

We performed differential gene expression analyses in thirteen major cell types in which there were greater than 50 cells of a given cell type in more than 10 individuals with and 10 without AUD. We utilized a pseudobulk approach using the 143 samples, summing counts across cells within each sample for each cell type, with sex, age, and ethnic origin as covariates. Samples were removed on a cell type-specific basis if the sample contained less than 50 cells of that cell type (See Supplementary Table 7 for a summary of the number of pseudobulk samples created for each cell type).

Eight cell types each contained over 700 differentially expressed genes (DEGs) (adjusted *p* value (*padj*) < 0.2) (Fig. 3A, Supplementary Table 7). Most DEGs had small effect sizes (e.g., in astrocytes, the average absolute $\log_2$ fold change was 0.17). In each of these cell types, more genes had higher expression in individuals with AUD than had lower. Many of the DEGs were differentially expressed in multiple cell types. Notably, astrocytes and oligodendrocytes had 833 DEGs in common, and D1 and D2 neurons had 538 DEGs in common (Extended Data Fig. 4). The differences in gene

expression were weakly correlated (Pearson correlation) within different neuronal cell type and within different non-neuronal cell types (ranges = 0.1-0.83 for neuronal cell types and 0.05-0.27 for non-neuronal cell types) (Fig. 3B, Supplementary Table 8). AUD-related expression differences within D1 and D2 neurons were more highly correlated (r = 0.83). However, D1/D2 neurons were much less correlated with either D1 or D2 neurons (r = 0.41 and 0.39 respectively).

Gene set enrichment analysis using pathways from the Reactome database[26] showed that genes that differ in expression with respect to AUD were enriched in hundreds of pathways in many cell types (Fig. 3C, Supplementary Table 9). Successive hierarchical and manual grouping of pathways revealed that many immune response pathways – such as the adaptive immune system, innate immune system, and cytokine signaling in immune system – were enriched in cells from individuals with AUD in multiple cell types. In individuals with AUD, DEGs in oligodendrocytes were enriched for several pathways associated with synaptic regulation and depolarization, such as “Neurotransmitter Receptors and Postsynaptic Signal Transmission” and “Voltage Gated Potassium Channels”. D1/D2 and FS neurons had decreases in gene expression within pathways reacting to translation and metabolism.

AUD-Associated Differences in Chromatin Accessibility

For cells in which both gene expression and chromatin accessibility information was available, the chromatin accessibility (combined reads for each cell type, see Extended Data Fig. 5 for cell type distribution for snATAC-seq cells) of several cell type-specific genes were plotted for the region surrounding the transcription start sites (TSS) (Extended Data Fig. 6). The chromatin accessibility signal for each cell type, which included cells from individuals with and without AUD, showed a strong signal near the TSS of its respective marker genes. The open chromatin regions (peaks) in each cell type showed varying degrees of similarity. Thirty-six percent of all open chromatin regions were shared among neuronal and non-neuronal cell types, while 34% of all peaks were unique to neurons and 30% unique to non-neurons (Fig. 4A). D1 neurons and D2 neurons had very similar open chromatin regions (Jaccard index = 0.8) while having less similarity with D1/D2 neurons (Jaccard index = 0.47). Astrocytes, oligodendrocytes, and OPCs had moderately similar open chromatin regions, with Jaccard indices of approximately 0.4 between these cell types (Fig 4B, Supplementary Table 10).

To determine the AUD-associated differences in chromatin accessibility for each cell type, we calculated the differentially accessible chromatin regions (DARs) – i.e., open chromatin regions that differed in accessibility between individuals with AUD and those without, again using a pseudobulk approach with the same 143 samples and the same covariates. Samples were removed on a cell type-specific basis if the sample contained less than 50 cells of that cell type (See Supplementary Table 12 for a summary of the

number of pseudobulk samples created for each cell type). We identified DARs for eight cell types (Supplementary Table 12); of those cell types, only oligodendrocytes, astrocytes, D1 neurons, and D2 neurons had over 50 DARs (*padj* < 0.2) (Fig. 4C). Just as with the DEGs, most of the differences were in the positive direction – chromatin becoming more open on average in samples from AUD individuals. However, most of these chromatin accessibility differences were relatively small – only in oligodendrocytes did any DARs surpass an absolute $\log_2$ fold change of 0.5.

We compared the magnitude and direction of chromatin accessibility differences to the gene expression differences in genes that had at least 1 DAR in the promoter. The AUD-associated DARs and DEGs were in the same direction for most genes in the four largest cell clusters (Fig. 4D-G). (88%, 90%, 73%, and 77% in oligodendrocytes, astrocytes, D1 neurons, and D2 neurons, respectively). Genes containing positive DARs were enriched among DEGs (with a positive enrichment score) in all four cell types (oligodendrocytes, astrocytes, D1 neurons, and D2 neurons; *padj* < 1e-8). The genes containing negative DARs were also enriched (with a negative enrichment score) among DEGs in astrocytes, oligodendrocytes, and D1 neurons. These results together imply that AUD-associated differences in chromatin accessibility are largely associated with a corresponding change in *cis*-gene expression.

Identifying Driver Genes for AUD by Integrating Differential Expression, GWAS, and Cell Type-Specific eQTLs

To identify the genetic component of differential gene regulation, we performed an integrative analysis using eQTL identification for each cell type and publicly available data. Several GWAS have identified loci associated with AUD-related traits: 496 independent loci statistically associated with number of drinks per week,[3] and 90 independent loci associated with problematic alcohol use[5], including 5 loci associated with both traits. These loci overlapped with the genomic locations of 3,406 and 749 genes, respectively, of which 147 were associated with both traits, making 4008 unique genes (Supplementary Table 13). Of these 4008 genes, 518 were differentially expressed (*padj* < 0.2) in astrocytes in our snRNA-seq data, 861 in oligodendrocytes, 318 in D1 neurons, and 329 in D2 neurons.

Of these GWAS-associated genes that were differentially expressed, those whose expression is also associated with a nearby genetic variant are even more likely to be potential driver genes for AUD (Fig 5A). We genotyped the 143 individuals using our snATAC-seq data, and tested variants overlapping cell type-specific open chromatin regions for an association with expression of nearby differentially expressed, for all cell types with at least one DEG (see Online Methods). In nine of the eleven cell types tested, we found at least one eQTL associated with a differentially expressed GWAS gene. Six cell types contained over 10 genes with an eQTL (Fig. 5B), and some genes contained eQTLs in multiple cell types. For example, *PPP2R3C,* within a locus

associated with PAU, was associated with an eQTL with a negative effect size at variant rs1056879 in oligodendrocytes, D1/D2 MSNs, and FS interneurons (Extended Data Fig. 7). *PPP2R3C* was expressed at lower levels in both cell types from individuals with AUD. Combined, these findings suggest that AUD is associated with downregulation of this gene's expression. *ADAL*, in a locus positively associated with alcohol drinks/week, was differentially expressed in D1, D2, D1/D2 and FS neurons, with a *cis*-eQTL at rs3742971 negatively associated with *ADAL* expression in all four of these cell types (Extended Data Fig. 7).

Genetic variants may be associated with a phenotypic trait (GWAS) and/or affect gene expression (eQTL). When the GWAS direction of effect of a variant is in the same direction as its association with expression of the gene is it proximally related to, we can infer that gene expression is positively associated with the trait, while opposite signs imply a negative association of expression with the trait. We further identified the genes in which this inferred effect correlated with differential expression findings by comparing the log fold change from our differential expression analysis to the GWAS effect size multiplied by the sign of the eQTL effect sizes for the same gene. We identified multiple genes in several cell types that did have expression changes in the same direction as the GWAS-eQTL effect, including *PPP2R3C* in oligodendrocytes and D1/D2 MSNs (Fig 5C-D), and *ADAL* in all MSNs (Fig. 5D-F). The expression of these genes was either positively associated with AUD (genes in the first quadrant) or negatively associated (i.e., the gene is protective for AUD, genes in the third quadrant).

Cell Type-specific Gene-Regulatory Mechanisms in AUD

To determine which transcription factors (TFs) and their target genes (TGs) become more or less active in AUD, we used LINGER, [27] a recently developed tool for gene regulatory network inference from paired single-cell expression and chromatin accessibility data (see Online Methods). After constructing the regulatory networks using pseudobulk data pooled across all cell types (using the same pseudobulk samples tested in the differential accessibility analysis, above), we extracted key TF-TG subnetworks (modules) from the network.

We detected 10 regulatory modules, each including several TFs and TGs from the pooled cell population *trans*-regulatory network (Fig. 6A). We detected differential expression in AUD individuals of module 2 genes in astrocytes, module 7 in D1/D2 MSNs (also marginally significant in oligodendrocytes, $p = 0.054$), and module 1 in microglia ($p < 0.05$). Several regulatory modules were significantly enriched for genes from the two GWAS studies utilized in our prior analysis. Modules 1, 2, 3, and 10 were enriched for genes associated with problematic alcohol use,[5] and modules 3 and 8 were enriched for genes associated with drinks per week.[3] Notably, genes in module 2 in astrocytes and in module 1 in microglia both had lower expression in individuals with AUD and were associated with problematic alcohol use. Module 1 contained only one

transcription factor, *ZBTB16*, which is a negative regulator of inflammation,[28] including in microglia.[29,30] Module 1 contained 6 target genes that were enriched for neurodegeneration in the Human Phenotype Ontology (HP:0002180, *padj* = 0.017), including *KLB*, a gene associated with alcohol consumption.[31]

Module 2 (showing lower expression in AUD in astrocytes) contained 24 TFs and 451 TGs. To determine which of these genes were more likely to be regulated together, we performed weighted gene co-expression network analysis (WGCNA[32]) of astrocyte single-nucleus data, which revealed ten groups of co-expressed genes (Supplementary Table 15). Co-expression group 3 (Co.E3) was enriched for differentially expressed AUD genes, particularly those with lower expression in AUD samples. There were 75 genes in Co.E3 overlapping with regulatory module 2 (Fig 6B), suggesting that these genes not only show similar expression patterns but also have similar patterns of regulation. Functional enrichment analysis identified several enriched pathways, including pathways from GO Cellular Component relating to glutamatergic synapses, and Nervous System Development and Negative Regulation of Wnt Signaling Pathways from GO Biological Process (Fig. 6C).

Next, we used the expression and accessibility of all target genes, based on the constructed trans-regulatory network, to identify key regulatory TFs in each cell type underlying the epigenetic and transcriptomic differences between control and AUD (called 'drivers' in the LINGER method, see Online Methods). Using the differences in chromatin accessibility and gene expression of target genes between individuals with and without AUD, we identified several key TFs associated with AUD in multiple cell types (Extended Data Fig. 8). In astrocytes, six TFs were identified as regulating AUD-related differences in both expression and chromatin accessibility, including the gene *JUND* (JunD proto-oncogene), identified as having increased regulatory activity in AUD in astrocytes.

Using chromVAR,[33] we identified 142 transcription factor motifs with significantly higher enrichment in AUD individuals ($p < 0.05$). Based on structure and binding pattern, 15 of the top 20 motifs (by p-value) with significantly higher activity in cells from individuals with AUD were related to the bZIP family (Supplementary Table 16, $p <= 0.005$). The bZIP family of transcription factors contain a leucine zipper sequence and homo- and hetero-dimerize before binding to their DNA sequence.[34] One bZIP TF motif that had significantly higher motif enrichment in astrocytes from individuals with AUD is recognized by *JUND* ($p = 0.01$). We observed that astrocytes with high *JUND* motif activity were largely in regions with high complement component 3 (*C3*) expression, a marker of reactive astrogliosis.[35] There was higher expression of *C3* in individuals with AUD (1.65 fold, *padj* = 0.0007) (Fig. 6E).

We saw a modest decrease in expression of myelin basic protein (*MBP*), a major component of myelin, in oligodendrocytes from individuals with AUD (*padj* = 0.11). This decrease was especially pronounced in a small subset of oligodendrocyte cells: graph-based subclustering of oligodendrocytes cells revealed three major subclusters (Fig.

6G), one of which had significantly lower *MBP* expression than the other two (Fig. 6H). This cluster was also marked by high expression of *OLIG2* (Fig. 6H). As with the astrocytes, we used chromVAR to identify differences in motif activity and found 616 motifs with activity significantly associated with AUD ($p < 0.05$), including *OLIG2* ($p = 0.028$, Supplementary Table 17) (Fig. 6I). This gene was also implicated in the gene regulatory network constructed with LINGER as having increased regulatory activity in AUD, based on the chromatin accessibility of its target genes.

Several genes implicated in the gene regulatory analysis were also identified in our integrative GWAS-eQTL-differential expression analyses, as described above, including three target genes in astrocytes from regulatory module 2 – *BTBD3*, *LRRC4C*, and *PTBP2.* (Extended Data Fig 9). As these three genes are (1) differentially expressed in AUD, (2) part of a differentially expressed regulatory module identified in gene regulatory network analysis, (3) *cis* to a variant associated with gene expression, and (4) associated with drinks per week, they have strong evidence linking them as potential driver genes of alcohol consumption and/or AUD in the caudate.

Activated Microglia Induce Reactive Astrocytes and Oligodendrocytes

We used MultiNicheNet[36], an R package for differential cell-cell communication analysis using single-cell data with multi-sample, multi-condition designs, to identify changes in cell-cell signaling between microglia, astrocytes, and oligodendrocyte cells and the downstream targets of these signaling events. The package uses pseudobulk differential expression (using the same pseudobulk samples tested in the differential expression analysis, above) of downstream target genes to infer changes in activity in upstream ligand-receptor signaling pathways between cell types. We identified three ligand-receptor pairs from microglia to astrocytes with high downstream gene activity: *IL1B-IL1R1*, *OSM-OSMR*, and *TNF-TNFRSF1A* (Fig. 6J see Supplementary Table 18 for all ligand-receptor pairs). These three pairs have been shown to work synergistically to induce pro-inflammatory cytokines in astrocytes[37]. Predicted downstream target genes of *IL1B-IL1R1* in astrocytes included *C3*, the widely used marker of reactive astrocytes, as well as bZIP family TFs *FOSL1*, *XBP1*, and *CEBPD.* We identified a single ligand-receptor pair from both astrocytes and microglia to oligodendrocytes with a high ligand activity: *TGFB1-ITGB8* (Extended Data Fig. 10).

Discussion

In this study, we present the first comprehensive profile at the single nuclei level of differences between individuals with and without AUD in gene expression, chromatin accessibility, and cell state in the caudate nucleus, and investigated potential regulatory mechanisms underlying these differences. We identified 17 distinct cell types in the caudate. Because of our large sample size, our comprehensive profiling enabled a more

granular and complete picture of the cell type landscape of the caudate, including rare interneuron and non-neuronal populations not identified in contemporary single-cell studies, such as a recent single-cell atlas of the brain[38]. These include a population of cholecystokinin/vasoactive intestinal polypeptide-expressing neurons detected in small numbers in animal models but previously not detected in the human striatum,[22] a population of calretinin-expressing neurons, knowledge of which has been extremely limited,[22] and a small cluster of vascular smooth muscle cells, a cell type which has recently been linked to neurovascular coupling[39]; a recent study has linked neurovascular coupling with chronic alcohol exposure in mice[40].

We identified thousands of genes differentially expressed in a range of cell types and characterized the accompanying differences in chromatin accessibility. The AUD-associated chromatin differences were correlated with expression differences, as expected. In every cell type, genes making up immune pathways – such as cytokine/interferon response, innate immune system, and complement cascades – were overrepresented among genes differentially expressed in the caudate from individuals with AUD. This extends previous findings that chronic alcohol exposure is associated with neurodegeneration and an increased neuroimmune response in both neurons and glial cells[41].

An increased proportion of microglia showed an inflammatory gene expression profile in those with AUD. Chronic alcohol exposure has been shown to cause microglial activation in mice, leading to neuroinflammation.[42] Indeed, gene regulatory network analysis revealed that *ZBTB16* is a key regulator whose expression is decreased in AUD. *ZBTB16* is known to counteract microglial M1 activation,[29] and its knockout in mice caused increased microglia and autism-like and schizophrenia-like behaviors.[30] Thus, the increased inflammatory response in microglia in AUD could be due in part to decreased *ZBTB16* activity. There is also evidence that the release of cytotoxic molecules associated with microglial activation may cause neuronal damage and contribute to neurodegenerative diseases.[43] Together, this suggests that the chronic inflammatory response in microglia could be in part driving AUD symptoms and changes in other cell types.

In astrocytes from individuals with AUD there was significantly higher expression of astrocyte reactivity marker *C3*. This extends to the caudate the previous evidence that inflammation evoked by ethanol exposure is accompanied by reactive astrogliosis.[8,44] Furthermore, the cells with increased *C3* expression also had significantly higher predicted activity of bZIP transcription factors such as *JUND,* suggesting that changes in these transcription factors may be regulating astrocytes as they undergo reactive astrogliosis. Gene regulatory network analysis identified a group of genes with similar patterns of *trans*-regulation that had decreased expression in AUD. These genes were overrepresented with gene sets related to glutamatergic synapses, consistent with previous work linking the disruption of glutamate homeostasis in astrocytes to AUD.[44] Other enriched pathways in these co-expressed and regulatory genes in astrocytes

include nervous system development and negative regulation of Wnt signaling. A recent study has also implicated the disruption of Wnt signaling in the striatum of rats as an effect of high cocaine self-administration[45]. Together this suggests that decreased regulation of Wnt signaling, especially in astrocytes, may play an important role in addiction.

In oligodendrocytes, we observed differences in expression and chromatin accessibility in thousands of genes, and enrichment in biological pathways relating to neurotransmitter uptake and depolarization. We also observed that the gene encoding myelin basic protein had slightly, but significantly, lower expression in individuals with AUD. There is evidence that action potential propagation through axons can be regulated by oligodendrocyte depolarization.[46] In pathological conditions such as excitotoxicity, excessive neurotransmitter release from neurons can lead to an excessive intracellular Ca^{2+} flux into oligodendrocytes, damaging myelinating processes.[47] Lower *MBP* expression was limited to cells marked by higher expression of *OLIG2* (Fig 6G-H). *OLIG2*, a master regulator in mature and developing oligodendrocytes, has been shown to have higher activity after brain injury,[48] and has been extensively linked to myelination: one study found that replacing *Olig2* with its dominant-active form in rodents led to decreased expression of *MBP,*[49] and another study showed that deletion of the *Olig2* gene accelerated remyelinating processes.[50] This suggests that our observed increase in *OLIG2* activity in AUD individuals may be in part lead to dysregulation of myelination in oligodendrocytes.

Cell-cell communication analysis revealed that signaling involving proinflammatory molecules IL-β*,* TNF, and oncostatin M from microglial cells to astrocytes is higher in individuals with AUD, concordant with the hypothesis that activated microglia induce neurotoxic reactive astrocytes[35]. These three molecules have been shown to work synergistically in several cell types, including in astrocytes, to induce pro-inflammatory and neurotoxic molecules, such as nitric oxide[51] and prostaglandin E(2).[37] Although reactive astrocytes can induce death of neurons and oligodendrocytes, we did not observe a significant difference in relative proportions of neuronal cell types and oligodendrocytes between individuals with and without AUD. We found increased signaling via *TFGB1-ITGB8* from both microglia and astrocytes to oligodendrocytes. TGF-*β*1 signaling is known to increase after injury, and studies have shown that ethanol exposure induces TGF-*β*1 signaling in rats.[52,53] Previous work has shown that TGF-*β*1 expression increases in astrocytes and microglia in animal models of cerebral ischemia,[54] and another study has shown that TGF-β1 signaling plays a role in myelination in oligodendrocytes.[55]

We DEGs and DARs were highly correlated between D1- and D2-type medium spiny neurons, which are components of the direct and indirect pathways, respectively, of the basal ganglia. Similar biological pathways were enriched in individuals with AUD, such as pathways relating to RNA processing (‘RNA Metabolism’, ’Processing of Capped Intron-Containing pre-mRNA') and immune response (‘Innate Immune System’,

complement-related pathways). Recent studies have also found dysregulation of neuroimmune genes in neurons in several brain regions in mice[56]. We observed a small cluster of medium spiny neurons expressing both D1 and D2 dopamine receptor genes. This MSN type, variously described as eccentric MSNs, D1H, and D1/D2 hybrid MSNs,[25,57] has been observed in mice,[57,58] primates,[25] and humans,[59] but its association with AUD has thus far been unknown. The pattern of gene expression changes in these neurons was less correlated with the other MSN types and different biological pathways were enriched: 'HDMs Demethylate Histones' was the most highly enriched pathway in AUD individuals, while many metabolic and translational control pathways were negatively enriched, i.e., having lower than expected expression in AUD individuals. These differences from the classical D1 and D2 neuron types suggest that these neurons may play a distinct role in the caudate. Indeed, these neurons have been shown to be morphologically distinct from D1 and D2-type MSNs, with a smaller cell body, less expansive dendrite structure, and fewer spines, and were differently affected by treatment with a denervating agent, implying a complementary functional role,[25] which may explain the distinct pattern of differences we observed in this neuronal subtype.

Using GWAS data and eQTL identification, we found several genes in multiple cell types with strong evidence of being linked to AUD. For example, the variant rs1412825, located within a locus positively associated with drinks per week,[3] was negatively associated with expression of the gene *PPP2R3C* in both oligodendrocytes and D1/D2 MSNs. This, combined with our finding that PPP2R3C had significantly lower expression in oligodendrocytes and D1/D2 MSNs in AUD individuals, suggests that *PPP2R3C* could be protective for AUD. Interestingly, expression of *PPP2R3C* was recently shown to be significantly associated with problematic alcohol use in the nucleus accumbens – another part of the striatum – using a transcriptome-wide association analysis.[60] We observed a single variant, rs3742971, within a locus positively associated with problematic alcohol use,[5] that was negatively associated with expression of the gene *ADAL* in four neuronal cell types (D1 MSNs, D2 MSNs, D1/D2 MSNs, and FS interneurons). *ADAL* had lower expression in individuals with AUD in these cells. In mice, elevated *Adal* levels contribute to low alcohol preference.[61] This suggests that *ADAL* may be an important factor in the development of AUD.

Combining the above integrative analysis (differential expression + eQTL + GWAS) with gene regulatory network inference, we identified three genes in astrocytes with strong evidence of being key drivers of AUD. One of these, *BTBD3,* has been shown to regulate compulsive-like behavior in mice,[62] further evidence of this gene's potential importance in addiction.

There are several limitations to our study. Examining the caudate from individuals with and without AUD allowed us to identify differences in gene expression, chromatin accessibility, and pathways related to them. However, the nature of AUD does not allow us to differentiate between pre-existing genetic differences and those due to the chronic

alcohol consumption that is the hallmark of AUD. Another limitation is that those who drink heavily are more likely to smoke. A recent study found that 63.3% of drinkers at risk of alcohol dependence were smokers compared with 18.2% among drinkers not at risk, and 19.2% among non-drinkers.[63] Thus, some differences might be attributed in part to smoking. Finally, our results – being adjusted for ancestry status – do not capture the transcriptional and epigenetic diversity across ancestry group or measure the AUD-associated differences within specific ancestry groups. Indeed, a recent study found over 1,000 genes in the caudate nucleus whose expression is significantly associated with ancestry and 531 ancestry-dependent *cis*-eQTLs.[64]

In conclusion, we provide a detailed picture of the vast transcriptional and epigenetic differences between individuals with AUD and those without in many different cell types in the caudate nucleus and illuminate biological mechanisms underlying these differences and identify potential driver genes causing these differences in several brain cell types. Our work adds novel insights into the etiology associated with AUD, and points to key pathways and regulatory genes that are involved.

Acknowledgements:

The Collaborative Study on the Genetics of Alcoholism (COGA), Principal Investigators B. Porjesz, V. Hesselbrock, T. Foroud; Scientific Director, A. Agrawal; Translational Director, D. Dick, includes ten different centers: University of Connecticut (V. Hesselbrock); Indiana University (H.J. Edenberg, T. Foroud, Y. Liu, M.H. Plawecki); University of Iowa Carver College of Medicine (S. Kuperman, J. Kramer); SUNY Downstate Health Sciences University (B. Porjesz, J. Meyers, C. Kamarajan, A. Pandey); Washington University in St. Louis (L. Bierut, J. Rice, K. Bucholz, A. Agrawal); University of California at San Diego (M. Schuckit); Rutgers University (J. Tischfield, D. Dick, R. Hart, J. Salvatore); The Children's Hospital of Philadelphia, University of Pennsylvania (L. Almasy); Icahn School of Medicine at Mount Sinai (A. Goate, P. Slesinger); and Howard University (D. Scott). Other COGA collaborators include: L. Bauer (University of Connecticut); J. Nurnberger Jr., L. Wetherill, X., Xuei, D. Lai, S. O'Connor, (Indiana University); G. Chan (University of Iowa; University of Connecticut); D.B. Chorlian, J. Zhang, P. Barr, S. Kinreich, G. Pandey (SUNY Downstate); N. Mullins (Icahn School of Medicine at Mount Sinai); A. Anokhin, S. Hartz, E. Johnson, V. McCutcheon, S. Saccone (Washington University); J. Moore, F. Aliev, Z. Pang, S. Kuo (Rutgers University); A. Merikangas (The Children's Hospital of Philadelphia and University of Pennsylvania); H. Chin and A. Parsian are the NIAAA Staff Collaborators. We continue to be inspired by our memories of Henri Begleiter and Theodore Reich, founding PI and Co-PI of COGA, and also owe a debt of gratitude to other past organizers of COGA, including Ting- Kai Li, P. Michael Conneally, Raymond Crowe, and Wendy Reich, for their critical contributions. This national collaborative study is supported by NIH Grant U10AA008401 from the National Institute on Alcohol Abuse and Alcoholism (NIAAA) and the National Institute on Drug Abuse (NIDA).

Tissues were received from the New South Wales Brain Tissue Resource Centre at the University of Sydney which is supported by the University of Sydney and by the National Institute of Alcohol Abuse and Alcoholism (R28AA012725). Research reported in this publication was supported by the National Institutes of Health under Award Number U10AA008401. The content is solely the responsibility of the authors and does not represent the official views of the National Institutes of Health.

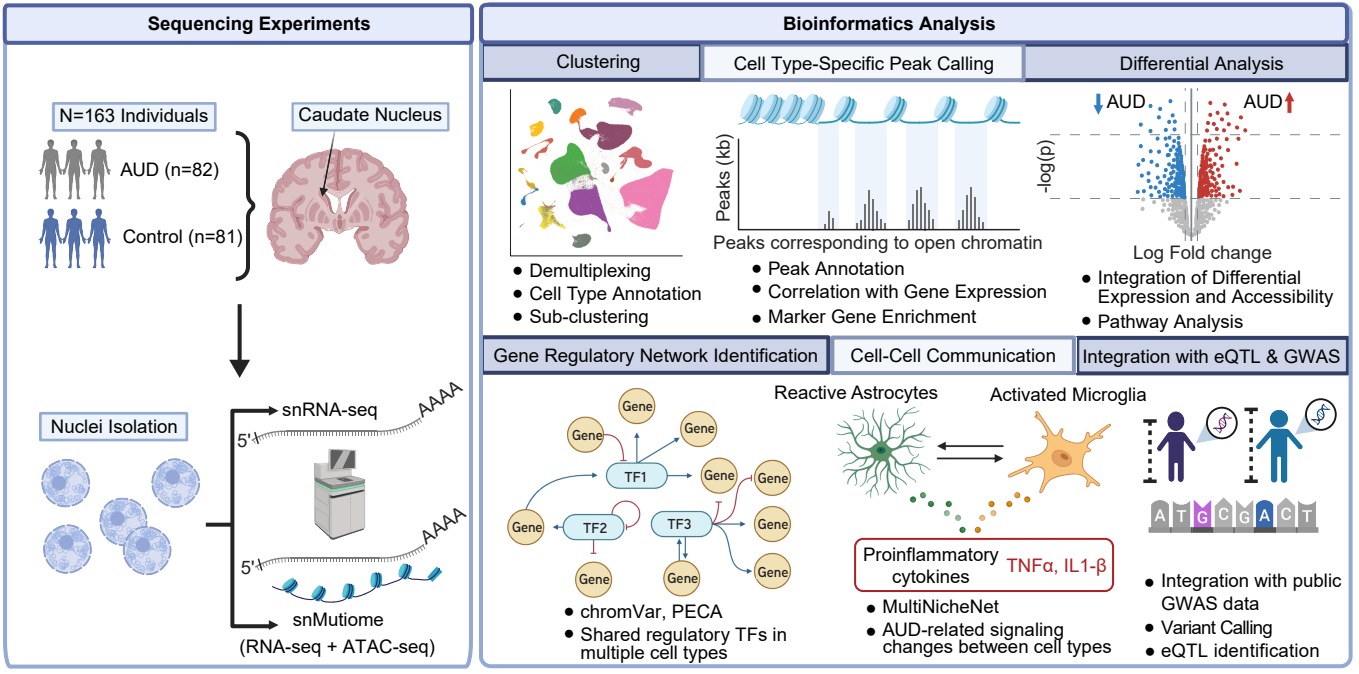

Figure 1: Scientific and Analytical Workflow. a, Experimental protocal: 10x HT assay and 10X multiome assay for 163 tissue samples of postmortem tissue samples from alcohol use disorder patients and controls. **b,** Informatics tools used. See Online Methods for details.

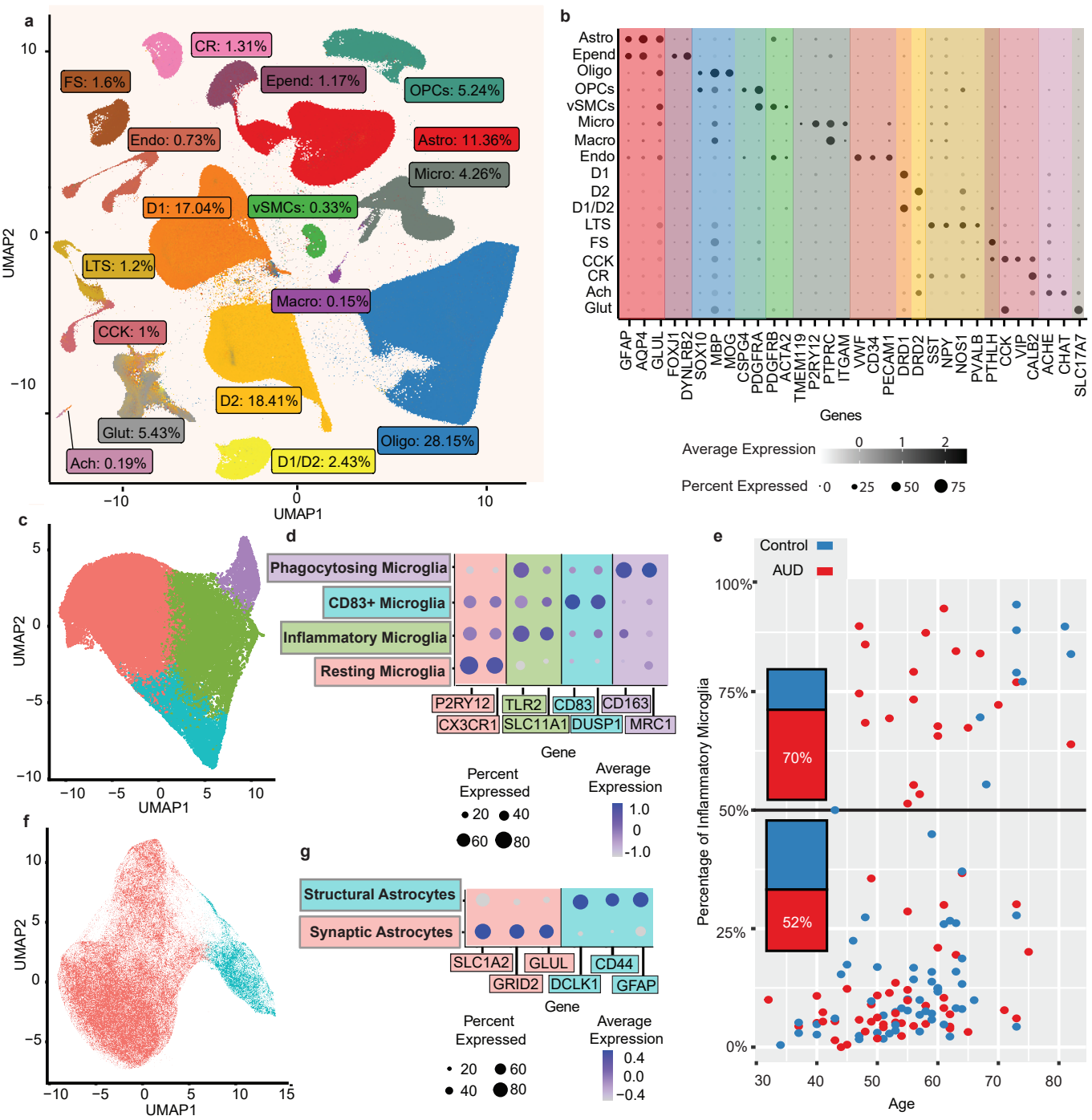

Figure 2: Cell Type Landscape of the Caudate Nucleus. a, UMAP visualization of 1,307,323 nuclei profiled in 10x multiome and 10x HT assays, visualization based on snRNA-seq profile. Cells are labeled by cell type and cell type proportion among all snRNA-seq cells. Cell types: Astrocytes (Astro), oligodendrocytes (Oligo), oligodendrocyte progenitor cells (OPCs), microglia (Micro), endothelial cells (Endo), vascular smooth muscle cells (vSMCs), non-microglial macrophages (Macro), D1-type medium spiny neurons (D1), D2-type medium spiny neuron (D2),medium spiny neurons expressing both D1 and D2 receptors (D1/D2), fast-spiking interneurons (FS), low-threshold spiking interneurons (LTS), calretinin-expressing interneurons (CR), and cholecystokinin-expressing interneurons (CCK), cholinergic neurons (Ach), and glutamatergic (Glut) neurons. **b,** Normalized expression in each cell type of the marker genes used to identify cell types. Size of dot corresponds to the percentage of cells expressing the gene; intensity of the dot indicates average gene expression level. **c,** UMAP of microglial cells, colored by sub-state. **d,** Dotpot of expression and prevalance of representative marker genes for each microglial sub-state. **e,** Scatter plot showing the age and proportion of inflammatory microglia of each sample, colored by AUD classification. Bars on the left show the percentage of AUD/control individuals among those with >=50% of microglia in the inflammatory state (above) and among those with <50% inflammatory microglia (below). **f,** UMAP of astrocyte cells, colored by subtype. **g,** Dotpot of expression and prevalence of representative marker genes for each subtype.

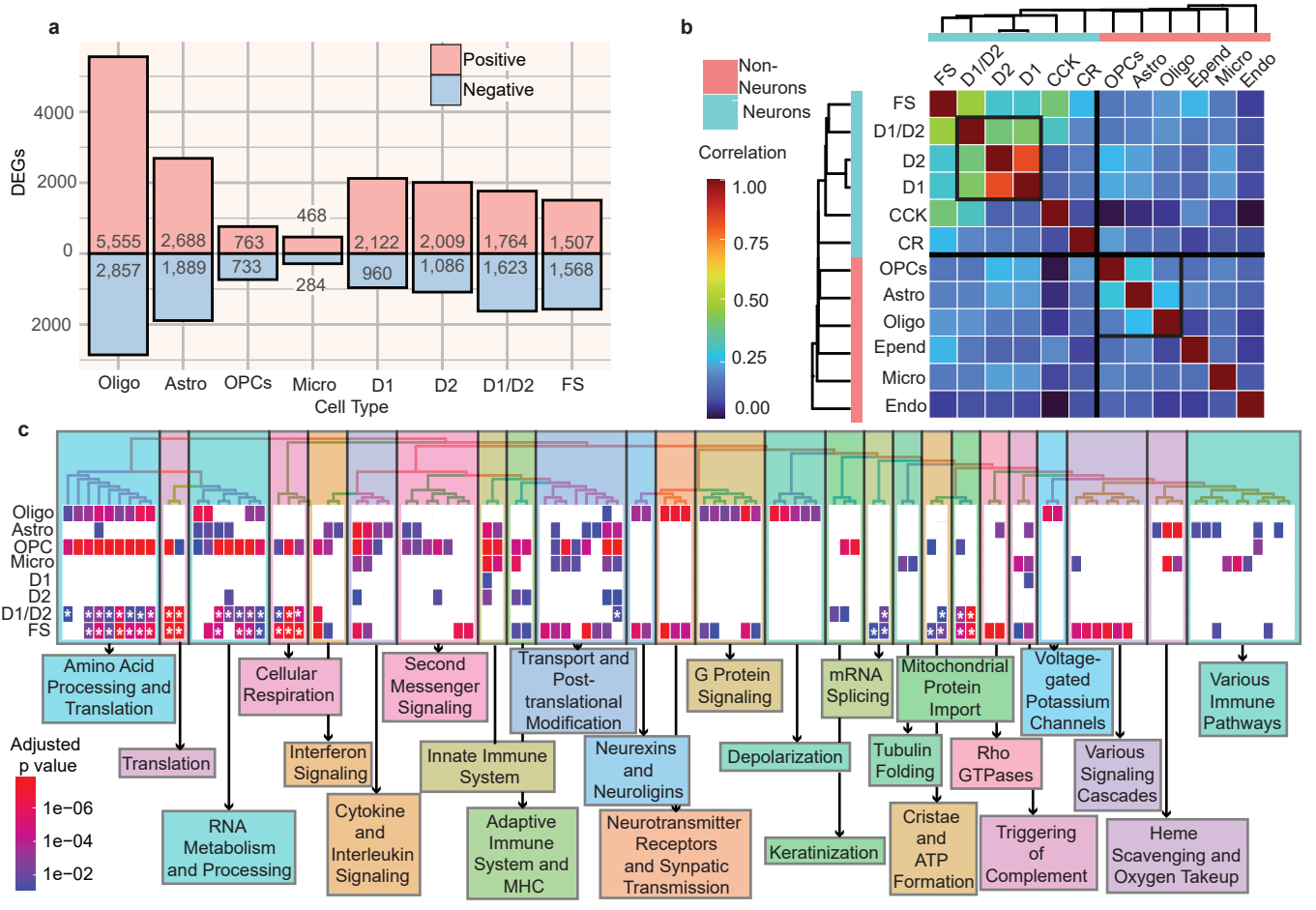

Figure 3: Characterization of AUD-associated Changes in Gene Expression in the Caudate Nucleus. a, Barplot showing number of genes differentially expressed in individuals with AUD for the eight cell types which have over 100 differentially expressed genes. Red and blue indicate positively and negatively differentially expressed genes, respectively. **b,** Heatmap of Pearson correlation of gene expression changes (log2 fold changes) between cell types, hierarchically clustered by Pearson correlation. **c,** Heatmap of biological pathways from the Reactome database enriched in AUD in each cell type. The top 100 enriched pathways (based on smallest FDR-adjusted p values) across all cell types are shown and were hierarchically clustered based on number of genes shared between the pathways. Heatmap cell color indicates FDR-adjusted p value. Asterick indicates negative enrichment score; all other pathways have positive enrichment scores. The pathways are divided into 25 clusters, which are manually labeled with a summary of pathways making up that cluster.

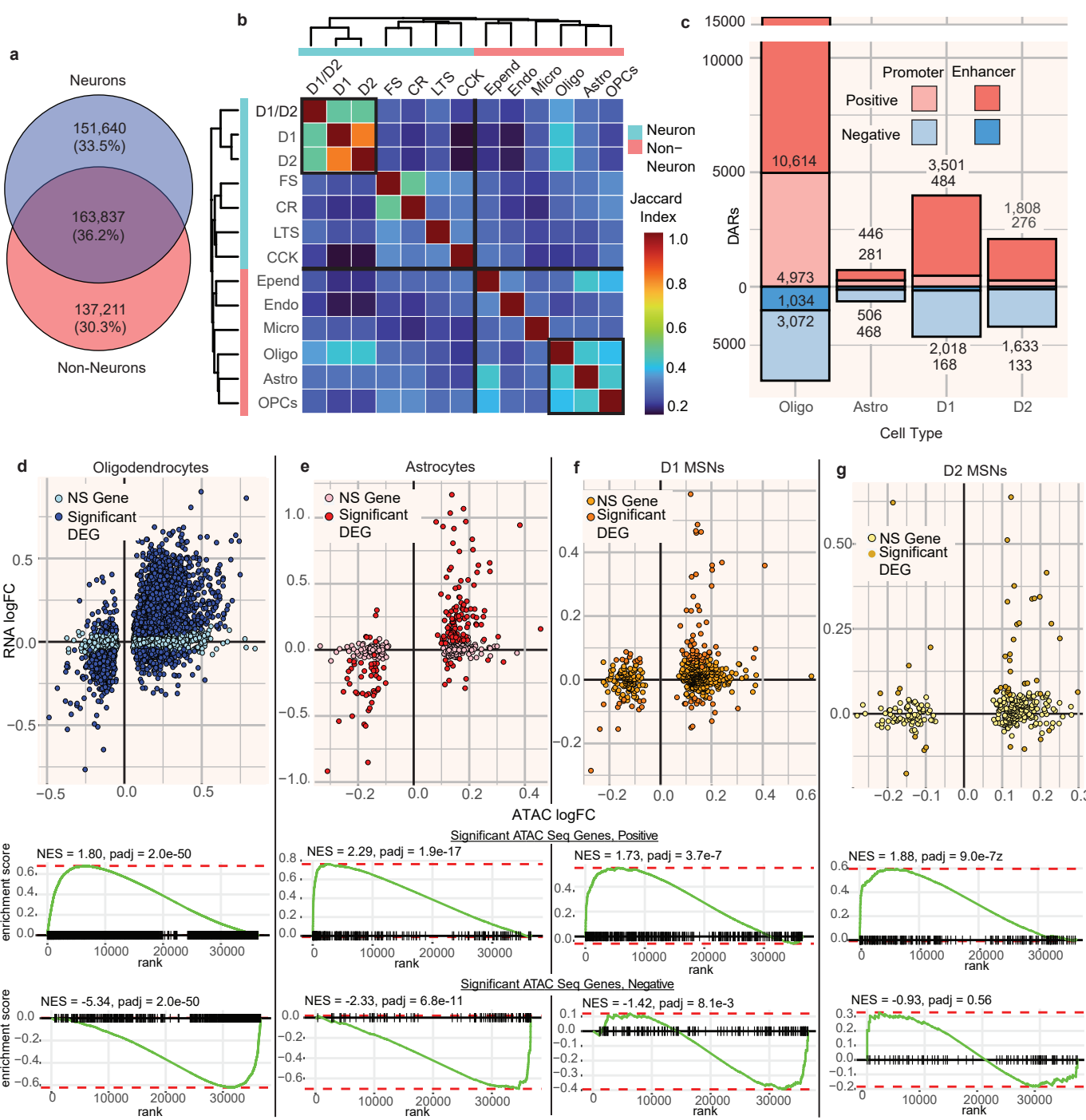

Figure 4: Characterization of AUD-associated Changes in Chromatin Accessibility in the Caudate Nucleus. a, Venn diagram of overlap between the union of chromatin accessibility peaks from all neuronal cell types and the union of peaks from all non-neuronal cell types. **b,** Heatmap of Jaccard similarity between cell types of the set of chromatin accessibility peaks, hierarchically clustered by Jaccard similarity. **c,** Barplot showing number of differentially accessible regions identified in oligodendrocytes, astrocytes, D1, and D2-type MSNs; red and blue indicate positively and negatively differentially accessible regions, respectively, and lighter and darker coloring indicate regions in promoter and enhancer regions of genes, respectively. Promoter regions defined as 1kb surrounding the transcription start side of each gene.**d,** Above: Scatterplot of log(2) fold changes of ATAC peak fold changes and gene expression fold changes for genes with at least one differentially accessible region (padj < 0.2), for oligodendrocytes. Genes are colored based on whether the gene is also differentially expressed (padj < 0.2). Below, GSEA plot of enrichment of the same ATAC-significant genes, split into two sets based on positive or negative effect size, across genes ranked by differential expression fold change. Normalized enrichment scores (NES) and FDR-adjusted p values (padj) for each GSEA test are shown. **e,** same as d, for Astrocytes, **f,** Same as d, for D1-type MSNs. **g,** Same as d, for D2-type MSNs.

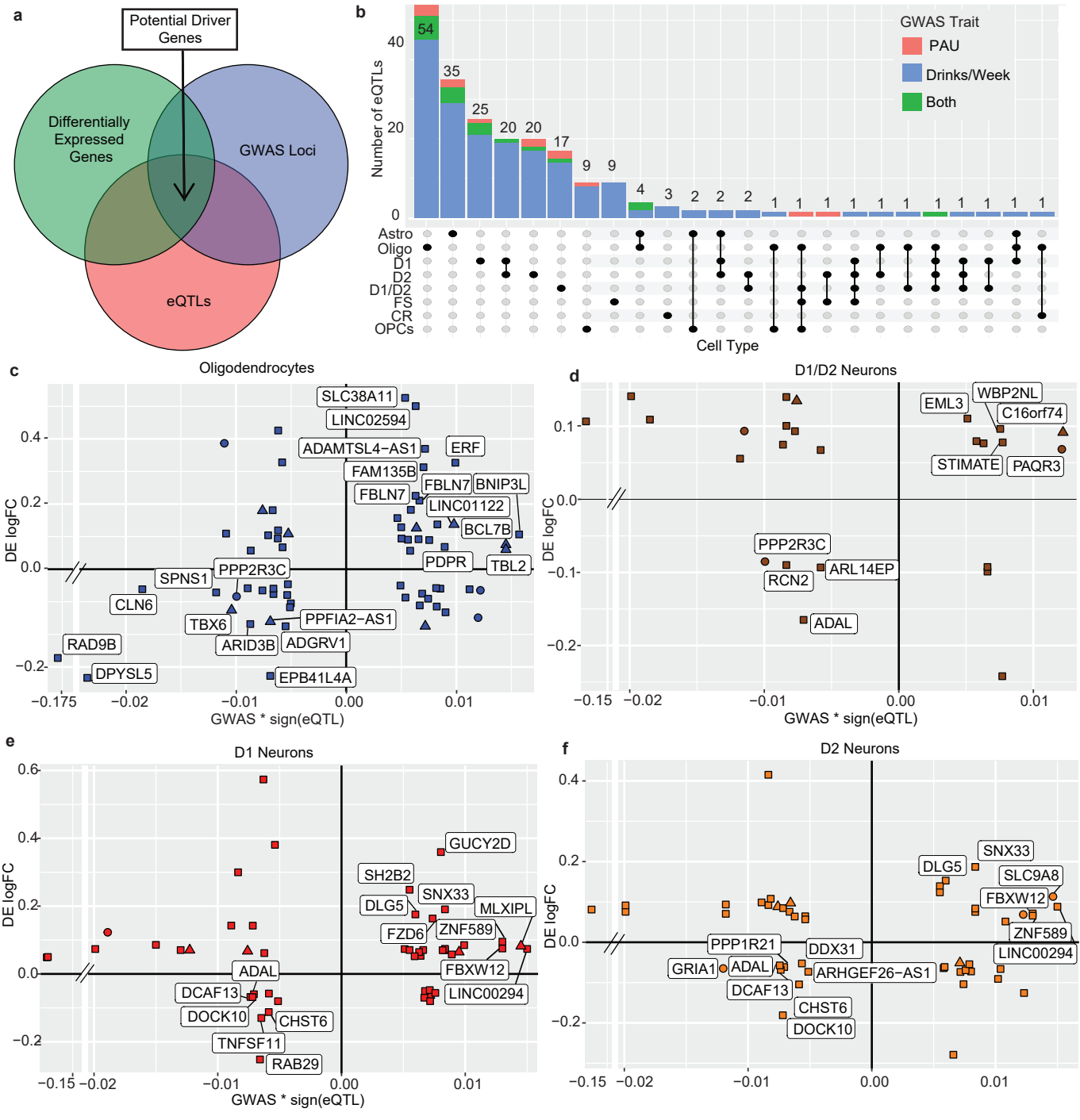

Figure 5: Integration of eQTL Analysis with GWAS Data and Differential Expression. a, Overview of DEG-GWAS-eQTL integration. Genes that are 1) Differentially expressed, 2) Contain a GWAS loci associated with an alcohol-related trait from public GWAS datasets, and 3) Contain an eQTL are more likely to be important driver genes in AUD. **b,** Upset plot showing number of differentially expressed genes (FDR < 0.2) containing a cis-eQTL (FDR < 0.2) and a GWAS loci for combinations of cell types. Colors indicate with which phenotypic trait the GWAS loci overlapping the gene is associated. PAU = Problematic alcohol use. **c,** For astrocytes, differential expression log fold change (AUD vs Control) plotted against GWAS effect size (using the variant within the loci with the smallest p-value), multiplied by the eQTL effect size, for each gene with a significant eQTL (FDR < 0.2). Shape indicates with which phenotypic trait the GWAS loci overlapping the gene is associated. PAU = Problematic alcohol use. **d, e, f,** as (c), for oligodendrocytes (d), D1 neurons (e), and D2 neurons (f).

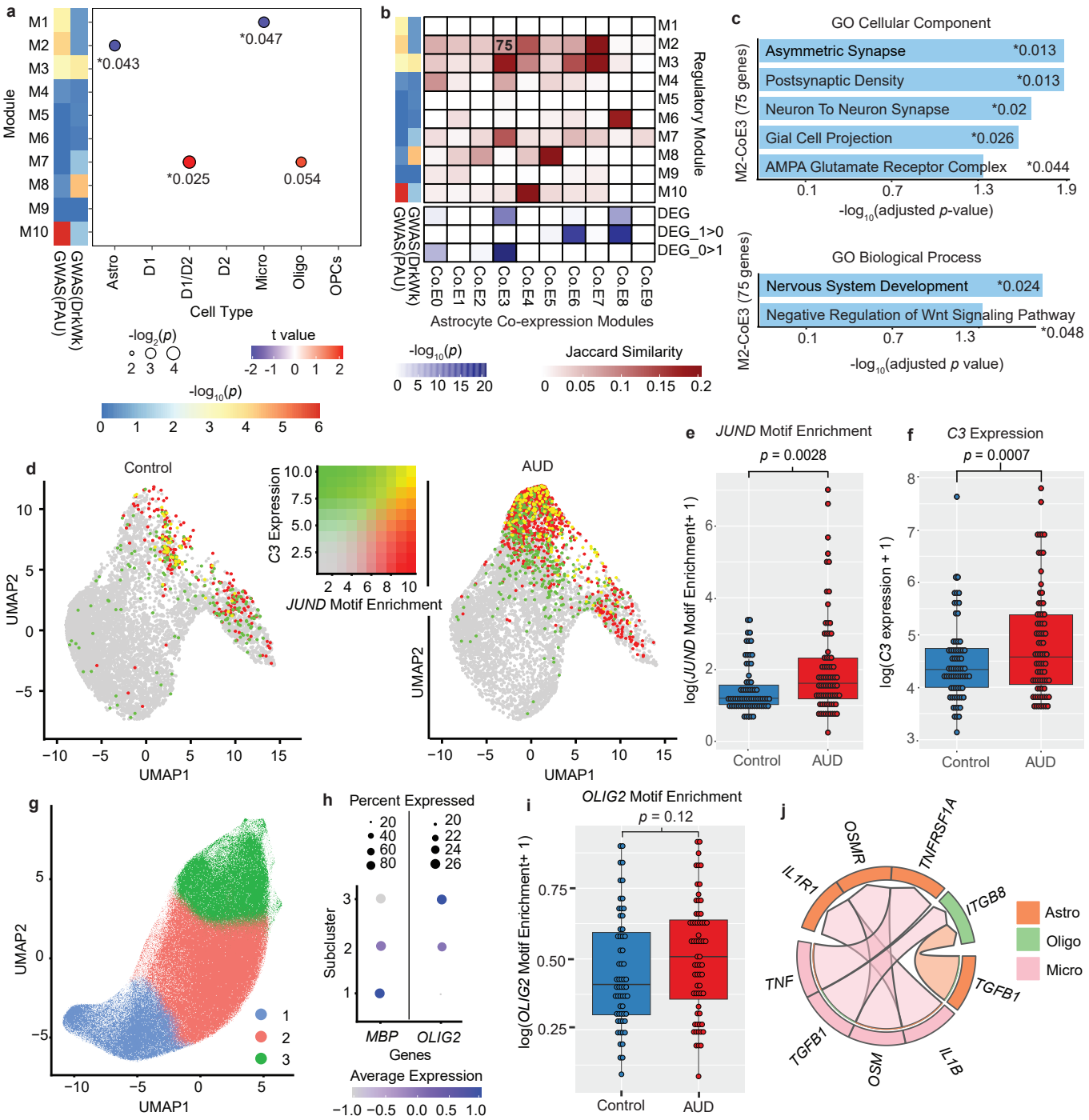

Figure 6: Cell Type-specific Gene Regulatory Networks Associated with AUD. a, Dotplot of the change in average expression between AUD and control samples of genes within 10 regulatory modules, as determined by gene regulatory network analysis in LINGER (see Methods). Size of dot represents p-value and color represents t-value of the difference in average gene expression. Left two columns display enrichment of module genes in the set of genes siginficantly associated with problematic alcohol use (left column, see Zhou, et al.) and drinks per week (right, see Saunders, et al.). **b,** Above: For astrocytes, heatmap showing Jaccard index between genes belong to the 10 regulatory modules, and 10 co-expression modules, as calculated by WGCNA (see methods). Below: For astrocytes, p-value of a t test, testing the difference of average expression of genes in each co-expression module, between AUD and control individuals. DEG_1>0 indicates higher expression in AUD indivuduals, and DEG_0>1 indicates higher expression in control individuals. Numbers in parentheses indicate number of genes belonging to each module, and bolded number indicate number of genes overlapping between the regulatory module and co-expression module. **c,** Functional enrichment results (GO:Cellular Component and GO: Biological Process databases) for the 75 genes overlapping regulatory module 2 and Co-expression module 3. Numbers marked by * indicates adjusted p-value of enrichment. **d,** UMAP of astrocyte cells split into cells from control and AUD indivuals, colored by JUND motif enrichment (red, as calculated by chromVAR, see Methods) and by log-normalized C3 expression (green). Yellow indicates high expression of C3 and high JUND motif enrichment. **e,** Boxplot of the log of chromvar motif activity score for the JUND motif for AUD and Control samples in astrocytes. **f,** Boxplot of the log of C3 gene expression for AUD and Control samples in oligodendrocytes. **g,** UMAP of oligodendrocyte cells, clustered and annotated into three subclusters using graph-based clustering. **h,** Dotplot of MBP and OLIG2 expression for each of the three oligodendrocyte subclusters. Size of dot indicates percentage of cells expressing the gene, and color of dot indicates average expression of the gene. **i,** Boxplot of the log of chromvar motif activity score for the OLIG2 motif for AUD and control individuals in oligodendrocytes. **j,** Circos plot showing the top five ligand-receptor interactions (determined by scaled ligand activity score from MultiNicheNet) between astrocytes, oligodendrocytes, and microglia.

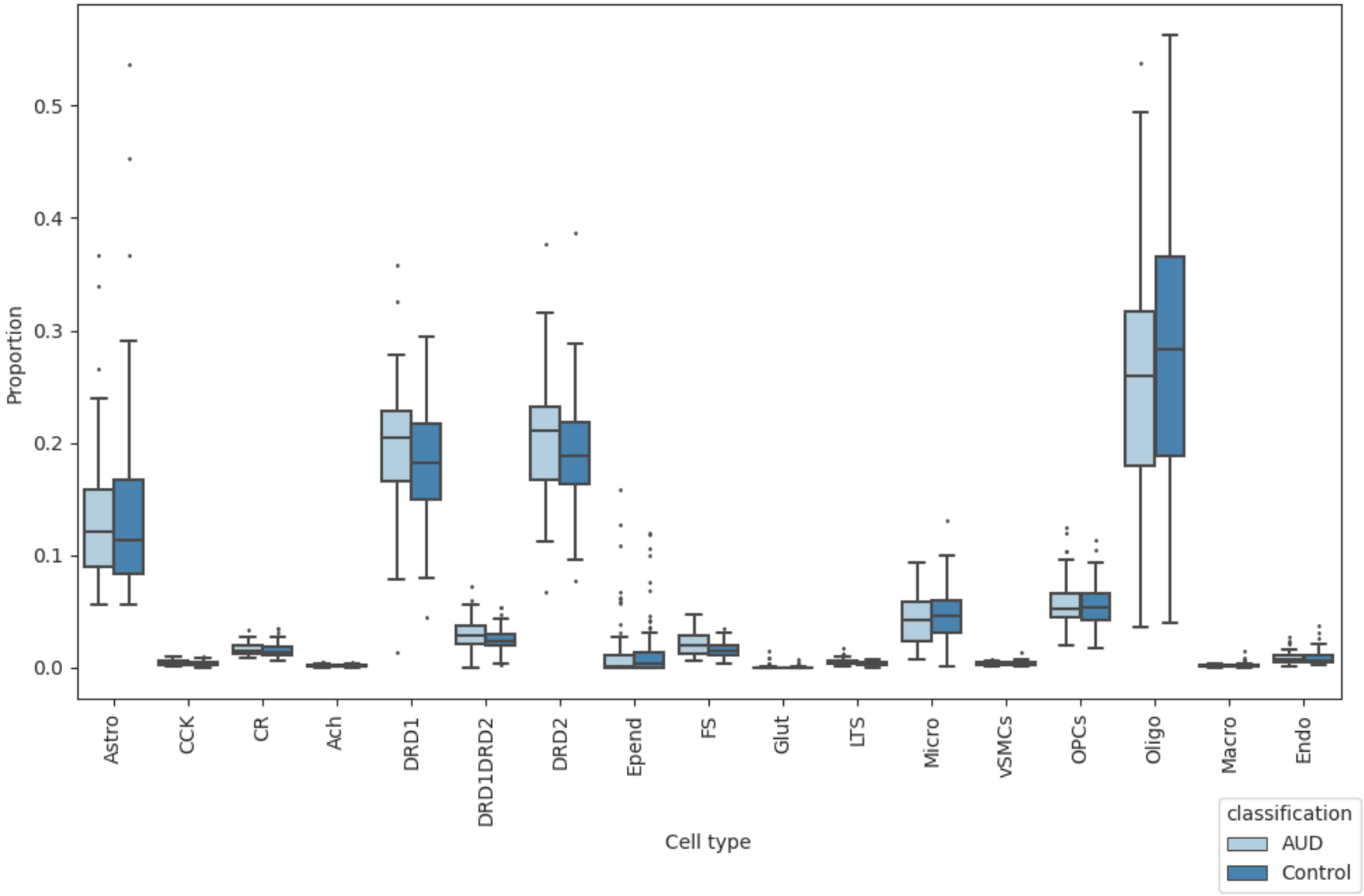

Extended Data Figure 1: Proportion of Each Cell Type for Each Sample, Grouped by AUD Classification.

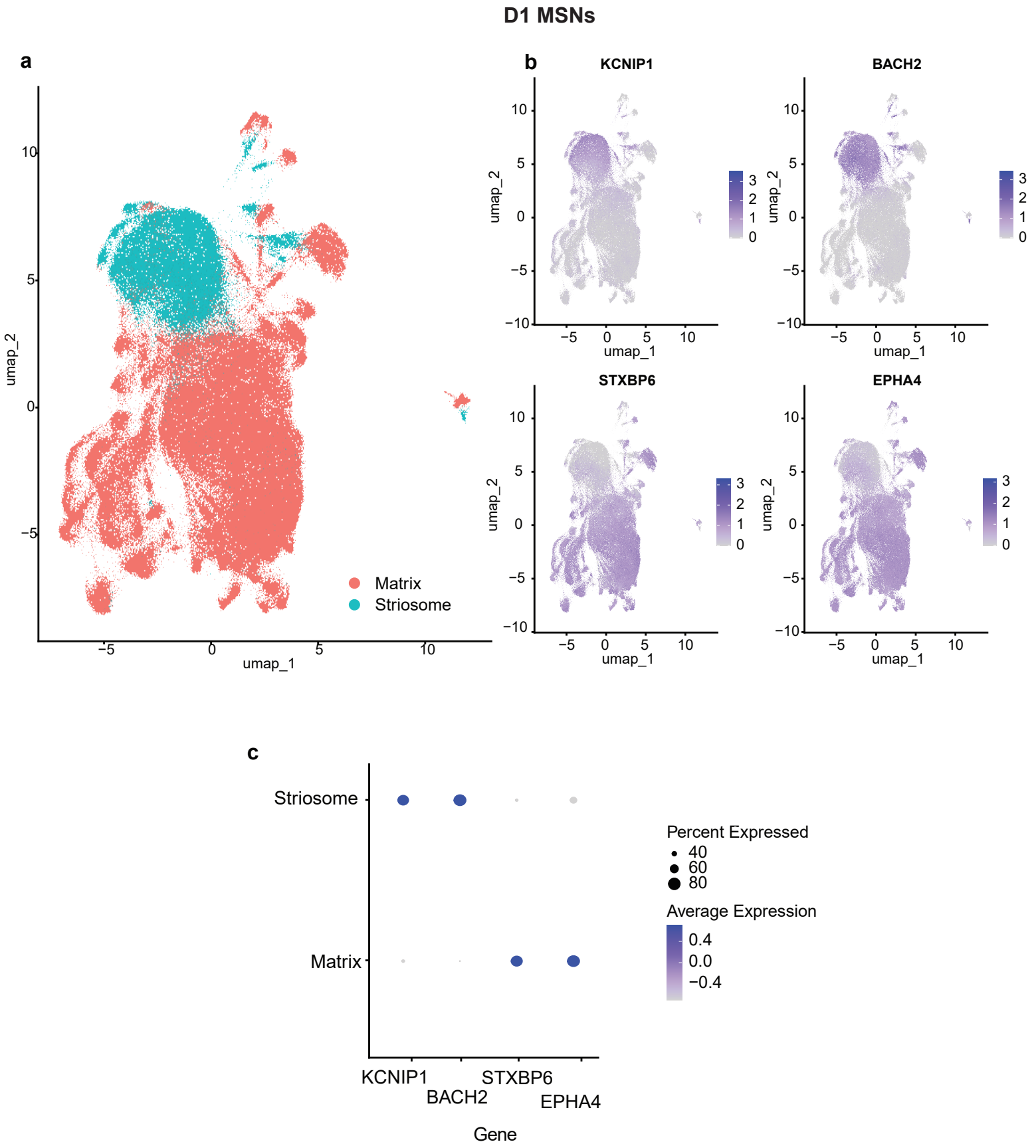

Extended Data Figure 2: D1 Medium Spiny Neurons Subtypes. a, UMAP of D1 MSN cells, colored by compartment (either matrix or striosome). b, UMAP of D1 MSN cells, colored by expression of marker genes used to assign compartment. c, Dotpot of expression and prevalance of representative marker genes for matrix and striosome compartments.

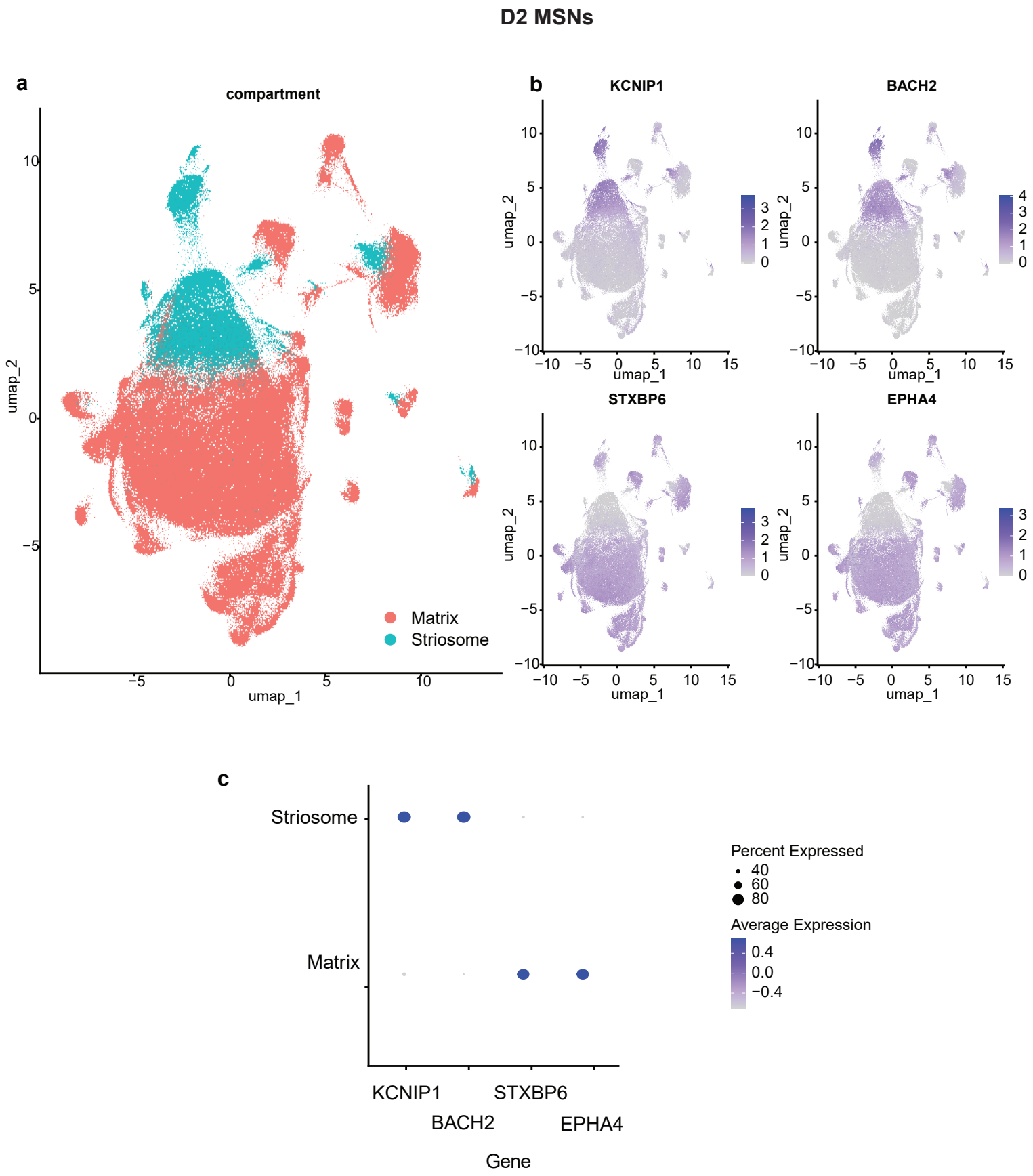

Extended Data Figure 3. D2 Medium Spiny Neurons Subtypes. a, UMAP of D2 MSN cells, colored by compartment (either matrix or striosome). b, UMAP of D2 MSN cells, colored by expression of marker genes used to assign compartment. c, Dotpot of expression and prevalance of representative marker genes for matrix and striosome compartments.

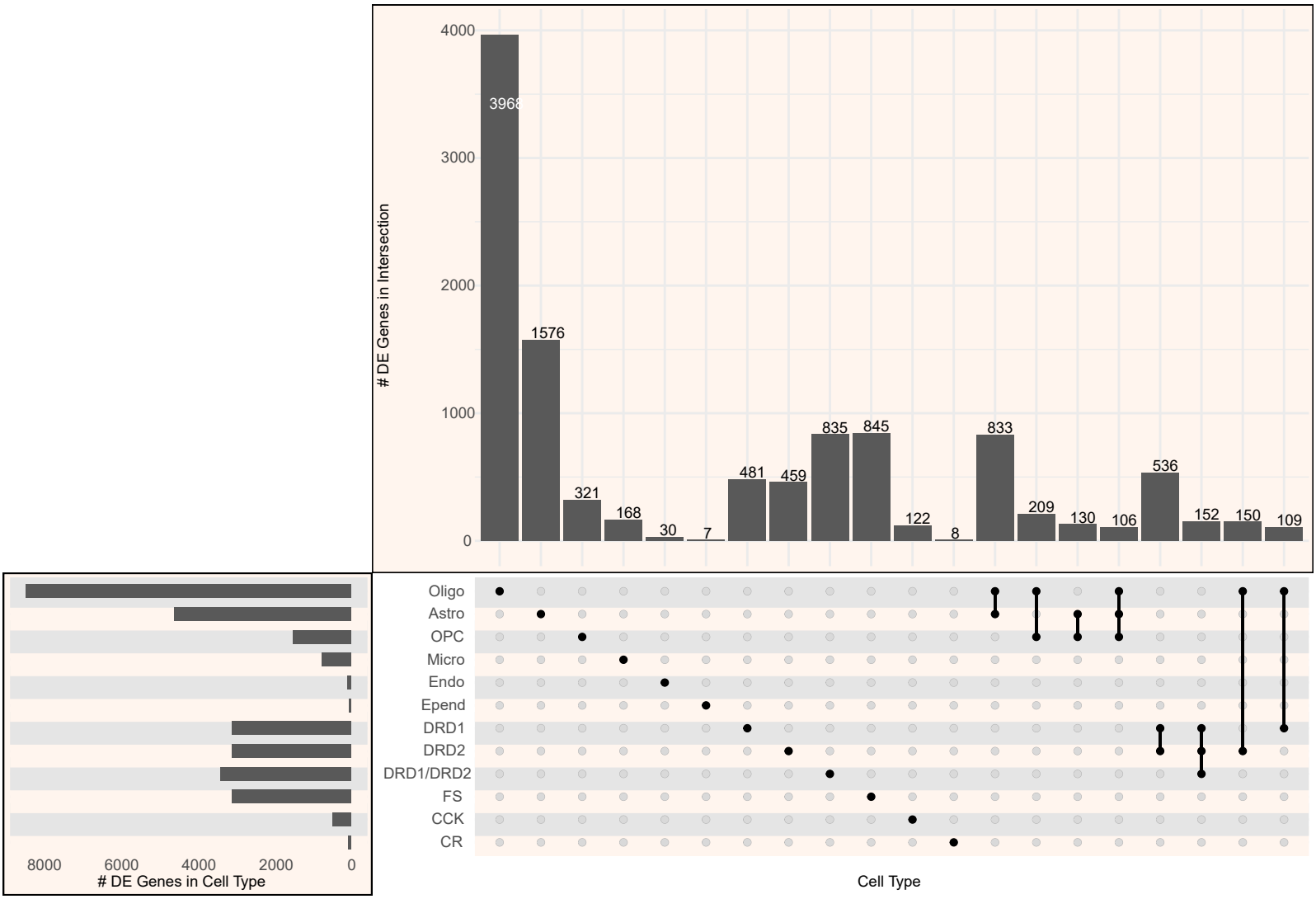

Extended Data Figure 4: Number of Differentially Expressed Genes in Multiple Cell Types. Upset plot shows the number of genes with expression significantly associated with AUD (padj < 0.2) in different combinations of cell types.

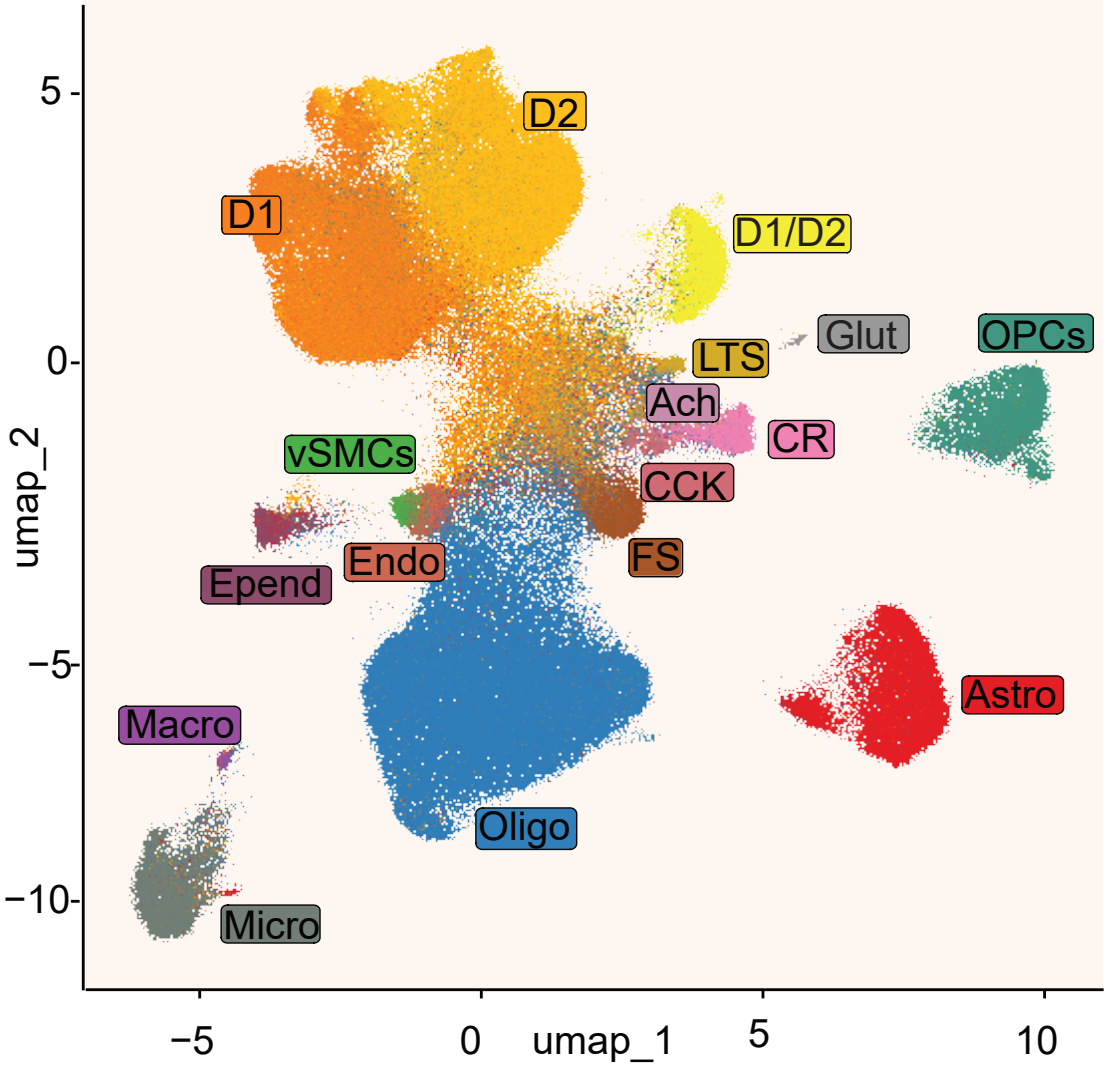

Extended Data Figure 5: snATAC-seq Cell Landscape. UMAP plotting each cell for which snATAC-seq data was available, clustered based on snATAC-seq data. Cell type labels for each cell was provided based on the cell's snRNA-seq data (see Fig. 2).

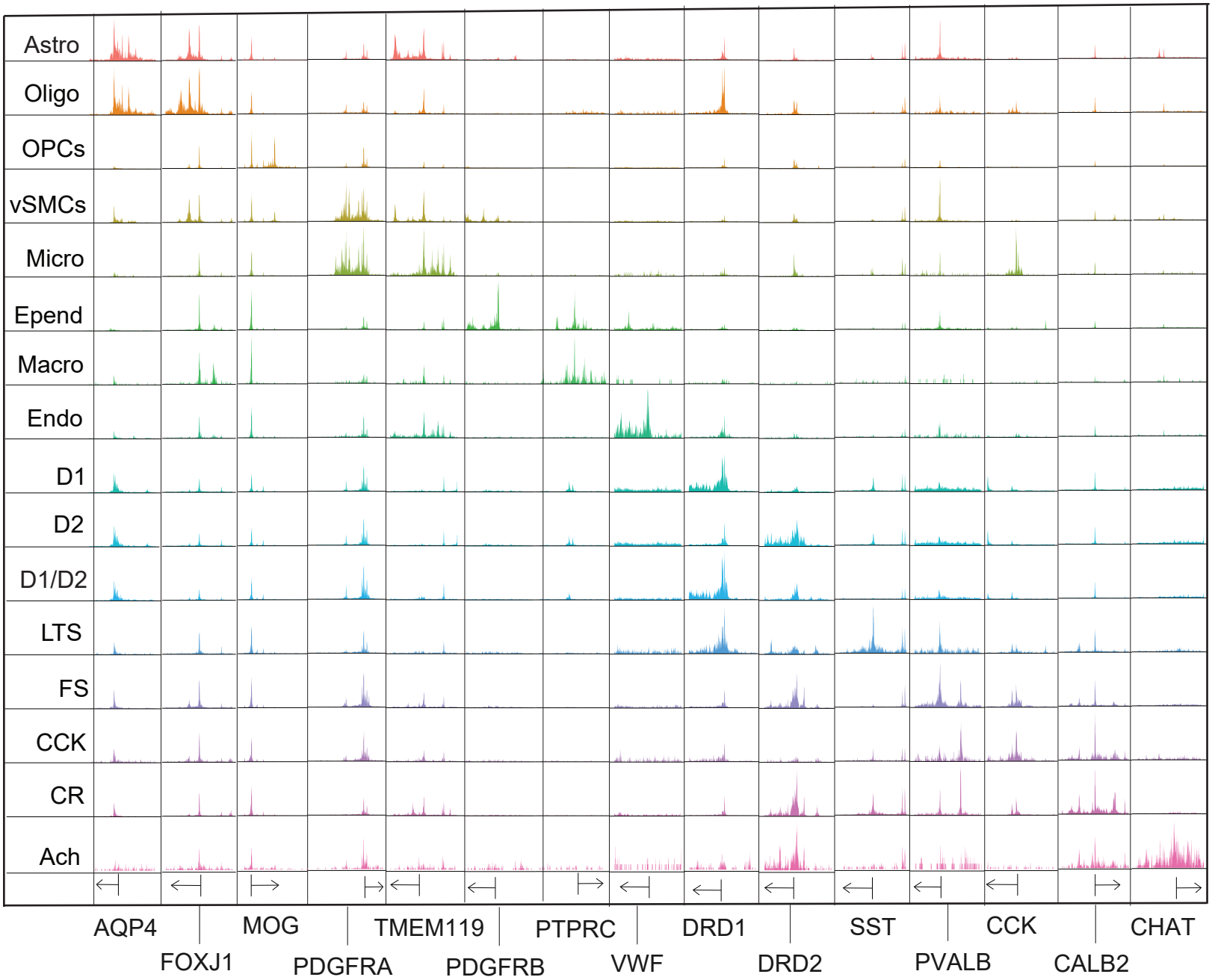

Extended Data Figure 6: Pseudobulk Accessibility Profiles for Each Cell Type at Canonical Marker Genes. 5kb on each side of the transcription start site of each gene are shown.z

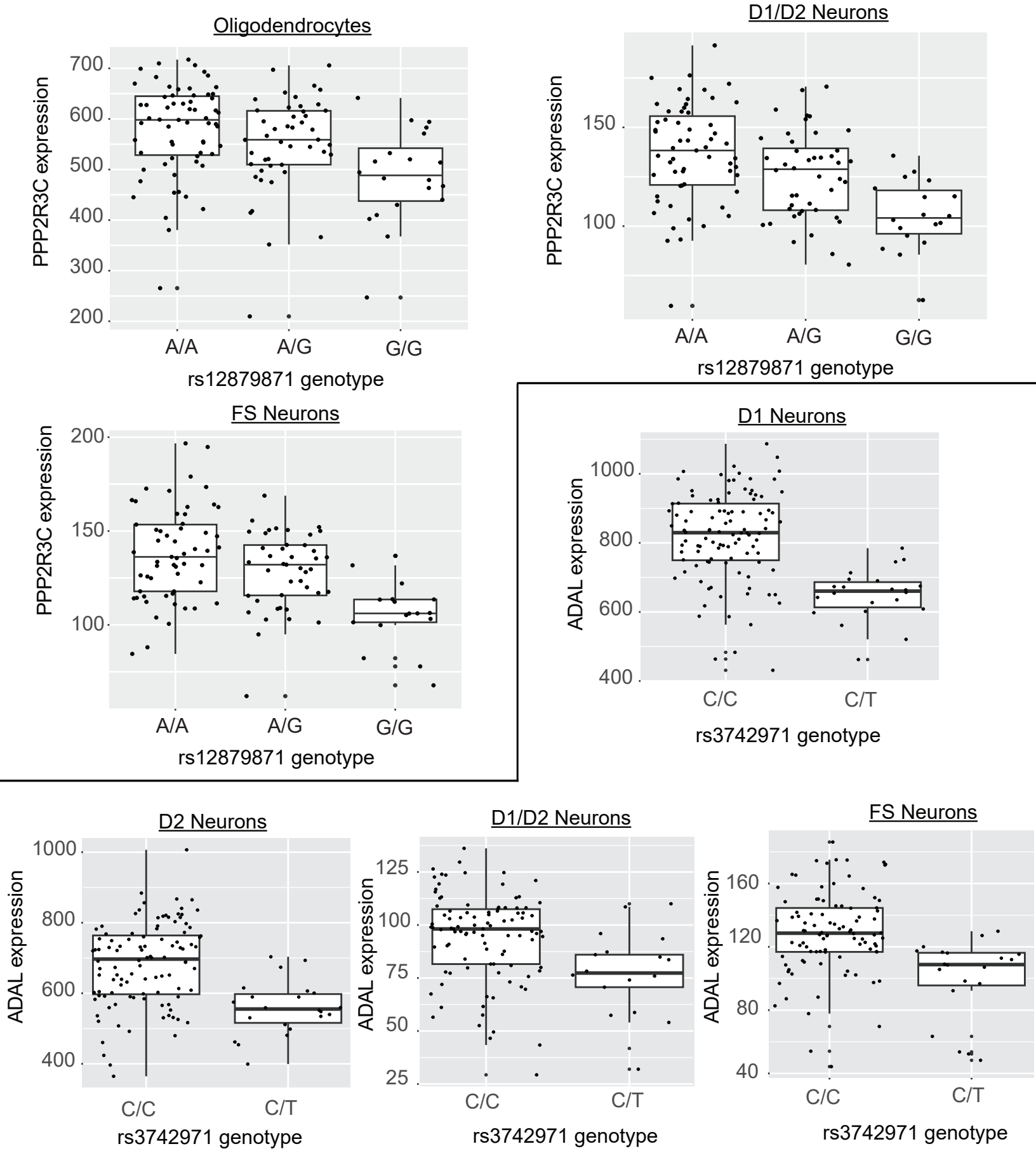

Extended Data Figure 7: Normalized Pseudobulk expression of PPP2R3C (above) and ADAL (below) for Each Sample. Plotted by genotype for the signficant eQTL in the cell types in which the eQTL was significant.

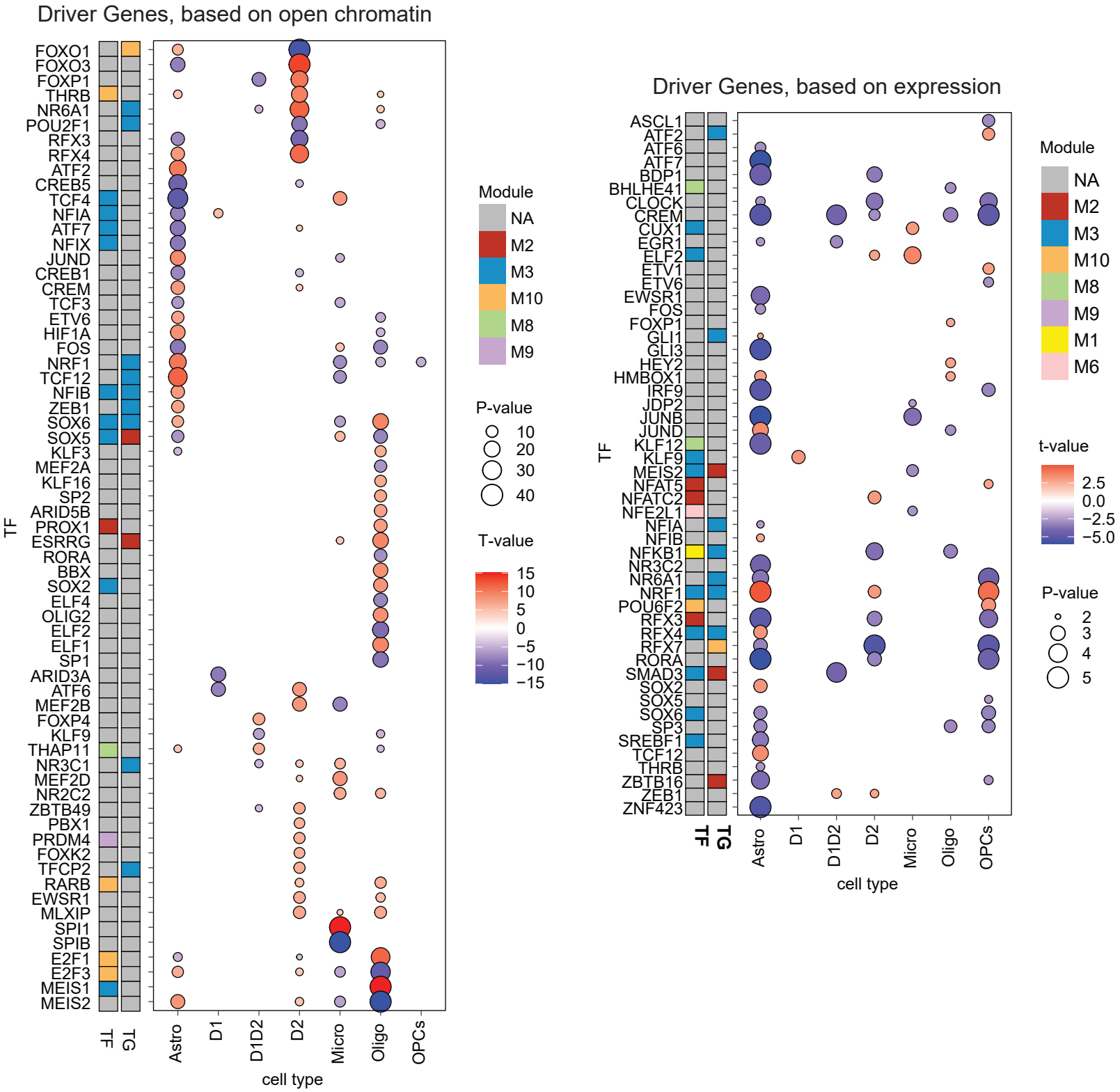

Extended Data Figure 8: Cell Type-specific Driver Gene Scores. a, Dotplot of all driver genes found, using LINGER's driver score, based on chromatin accessibility of target genes of that transcription factor. Size of dot correponds to p-value and color indicates t-value, of change in driver score between AUD and control individuals. Left two columns correspond to membership in regulatory modules. Genes ordered by cell type with most significant difference in driver score. **b,** Dotplot of all driver genes found, using LINGER's driver score, based on gene expression of target genes of that transcription factor. Size of dot correponds to p-value and color indicates t-value, of change in driver score between AUD and control individuals.Left two columns correspond to membership in regulatory modules. Genes are ordered alphabetically.

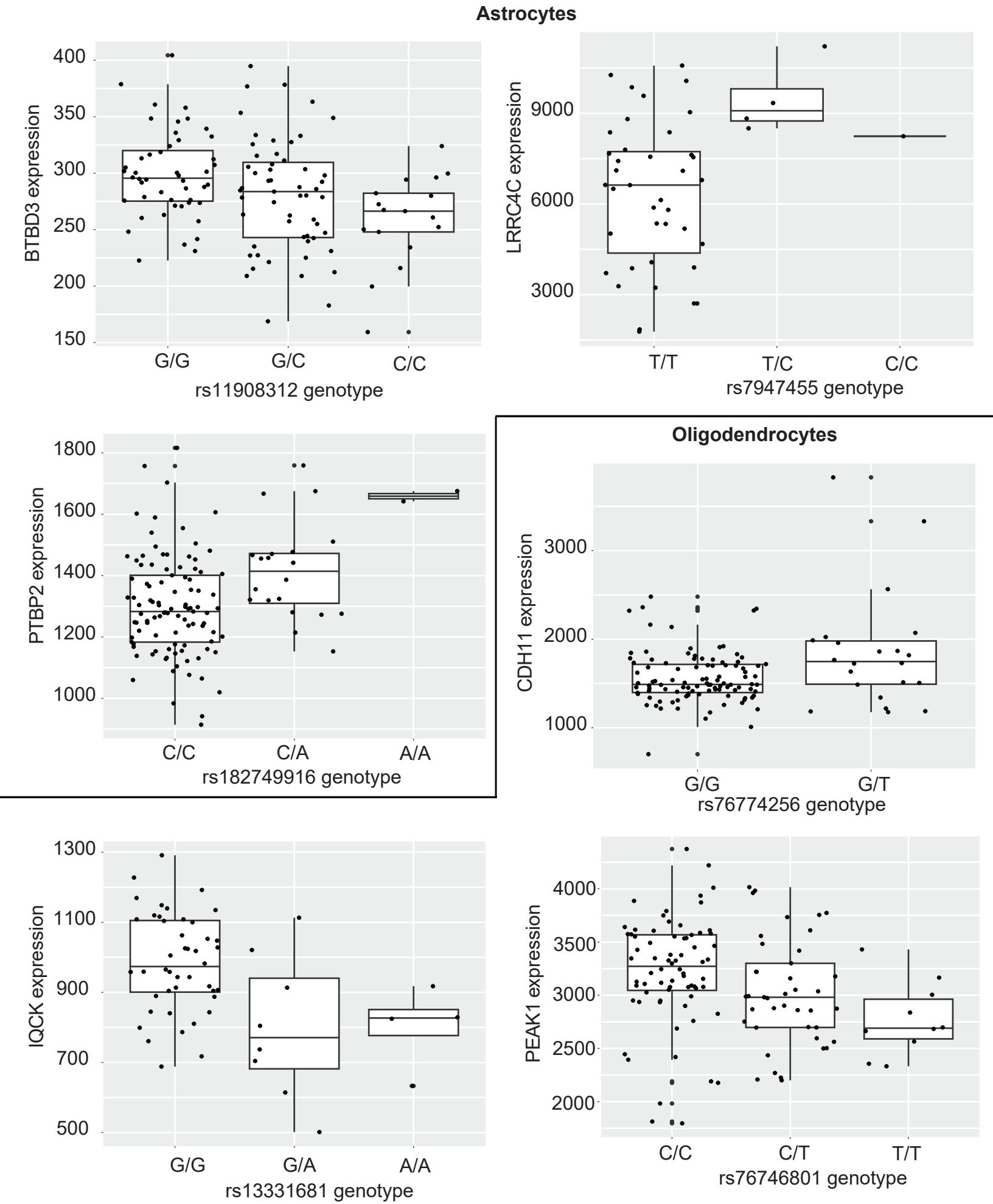

Extended Data Figure 9: Normalized Pseudobulk Expression of Target Genes with cis-eQTLs. Genes from modules 2 and 3 (as identified by LINGER) with a significant eQTL in astrocytes and oligodendrocytes. Plotted by genotype for the signficant eQTLs.

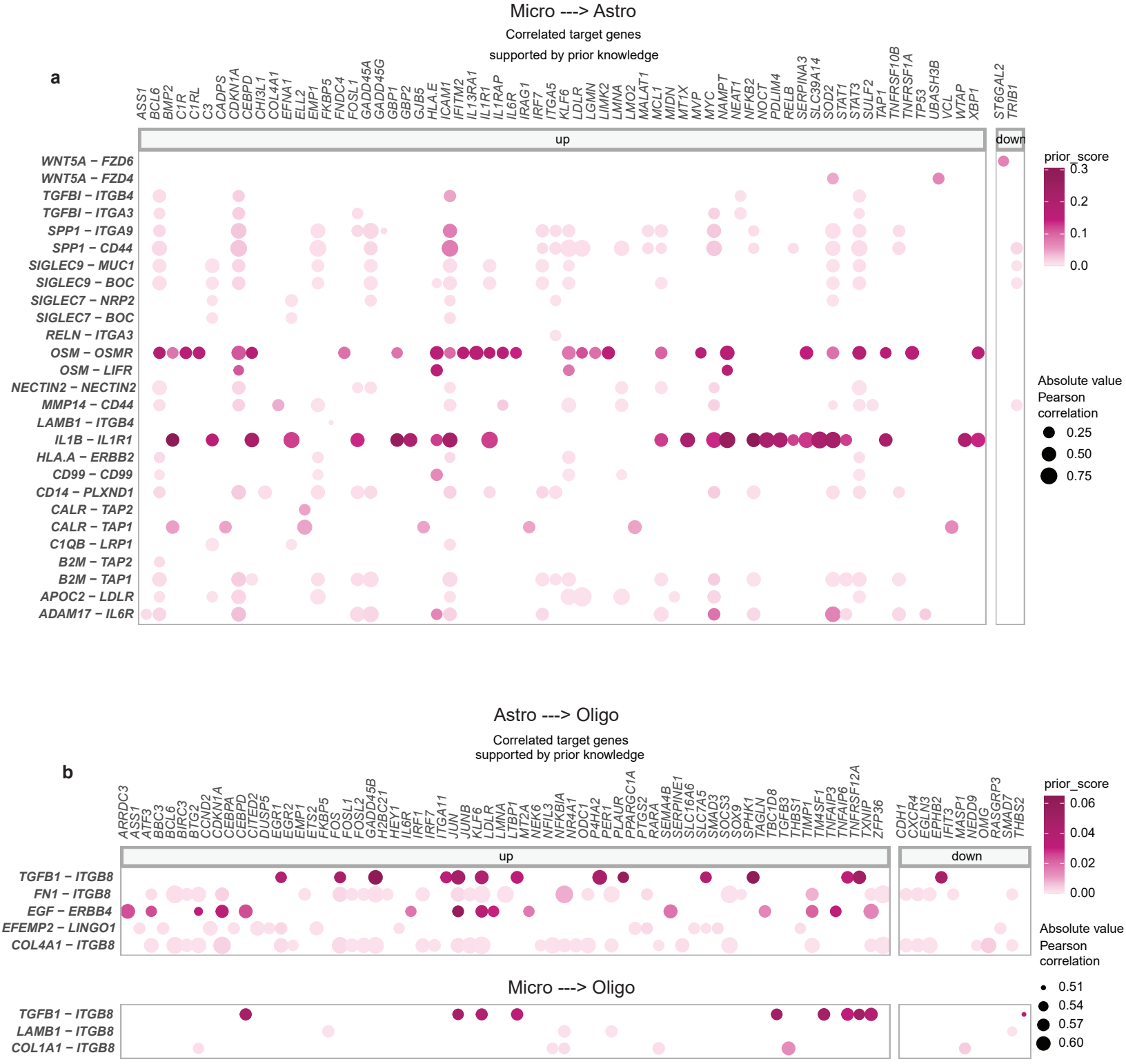

Extended Data Figure 10: Downstream Genes of AUD-associated Ligand-receptor Pairs. a. Microglia to astrocytes ligand-receptor pairs from MultiNicheNet cell-cell communication. All ligand-receptor pairs and target genes with high expression correlation (spearman or pearson > 0.50), having some prior knowledge to support their link (in the top 250 predicted target genes for the ligand, 'prior score' as predicted by MultiNicheNet), and being within the top 50 ligand-receptor pairs associated with AUD (as calculated by MultiNicheNet) are shown. Size of dots indicate pearson correlation between expression of ligand-receptor pair and target gene. Color of dot indicates prior score for link between ligand-receptor and downstream gene. **b,** As **a**, with astrocytes to oligodendrocytes pairs (above) and microglia to oligodendrocyte pairs (below)

Online Methods

Sample Collection

The caudate from post-mortem brains of 200 donors were initially included in this study. Tissue was obtained from the New South Wales Brain Tissue Resource Centre (NSWBTRC), University of Sydney, Australia (https://sydney.edu.au/nsw-brain-tissue-resource-centre).[65]

Genotype data processing and imputation

NSWBTRC samples were genotyped by using UK Biobank Axiom® Array (ThermoFisher Scientific, Waltham, MA, U.S.A.). Before imputation, palindromic SNPs and SNPs with genotyping rate <95%, minor allele frequency (MAF) <1%, or Hardy-Weinberg equilibrium P-value < 1E-4 were excluded. Genotype data was imputed by using the TOPMed Imputation Server.[66] Eagle v2[67] was used to phase the genotypes and Minimac4 v1.2.4[66] was used for imputation. Data from the Trans-Omics for Precision Medicine (TOPMed r3)[68] was used as the reference genomes.

Single-cell multiome assay

Nuclei Isolation for Single-cell Multiome

200 post-mortem caudate brain samples were utilized in the assay. The 200 specimens were divided into 25 pools, with 8 in each pool. The donors in each pool were both condition (control or AUD) and sex balanced. For each pool, around 20 mg tissue from each donor specimen was collected and combined into a sterilized 2 ml Dounce homogenizer. 2 ml chilled NP40 lysis buffer (10 mM Tris-HCl, pH 7.5, 10 mM NaCl, 3 mM MgCl2, 0.1% Nonidet P40 Substitute, 1mM DTT, 1 U/µl RNase inhibitor) was added to the Dounce homogenizer before the tissues were thawed. The tissues were homogenized 15x using pestle A, and 10x using pestle B, and were transferred into a centrifuge tube to incubate for 2 minutes on ice. After that, 2 ml wash buffer containing PBS, 1% BSA and 1 U/µl RNase inhibitor was added and mixed well. The lysed tissue was centrifuged at 500 rcf for 5 minutes at 4°C, then washed twice more with wash buffer and filtered through 70 µm and then 40 µm cell strainer separately. The pellet was resuspended in 2 ml wash buffer and mixed with 3.6 ml Sucrose Cushion Buffer I (nuclei PURE prep isolation kit, Sigma) containing 1 U/µl RNase inhibitor. 2 ml Sucrose Cushion Buffer I with 1 U/µl RNase inhibitor was added into one 15 ml Beckman Coulter centrifuge tube. After that, the 5.6 ml nuclei suspensions were gently added to the top of Sucrose Cushion Buffer I without mixing, and followed by centrifuging at 13,000 x rpm (30,000 rcf) (Beckman Coulter ultracentrifuge) with rotor SW40Ti for 45 minutes at 4°C. The purified nuclei pellet was washed by centrifuging at 300 rcf for 5 min at 4°C

with wash buffer, and the washed nuclei pellets was resuspended in wash buffer to target ~ 1000 nuclei/µl.

10X Single-cell Multiome Library Preparation and Sequencing

Paired ATAC and gene expression libraries were generated following the Chromium Next GEM Single Cell Multiome ATAC + Gene Expression User Guide CG000338_RevB (10X Genomics, Inc). In brief, the isolated nuclei from a pool of samples were first incubated in a transposition mix. The single nuclei master mixture containing tagmented single nuclei suspension was loaded into two well of a Next GEM Chip J, along with the single cell multiome gel beads and partition oil. The chip was then loaded to the Chromium X Controller for GEM generation and barcoding. Barcoded transposed DNA and cDNA were amplified after GEMs being released. At each step, the quality of cDNA, ATAC library and cDNA library was examined by Bioanalyzer 2000. The final single indexed ATAC libraries and the dual indexed gene expression libraries were sequenced on an Illumina Novaseq 6000, with index reads of 10 bp + 24 bp, and 100 bp paired-end reads.

Cell Ranger ARC Analysis

Cell Ranger ARC (cellranger-arc-2.0.0, http://support.10xgenomics.com/) was utilized to process the raw sequence data derived from the single-cell multiome libraries. Both the ATAC and gene expression FASTQ files were processed with the cellranger-arc count algorithm. The reference refdata-cellranger-arc-GRCh38-2020-A-2.0.0 (10x Genomics) was used. The filtered gene-cell barcode matrices and fragment files were used for further analysis.

Single-nuclei RNA-seq assay

Nuclei Isolation for Single-nuclei RNA-seq

170 post-mortem caudate brain samples (same individuals as in Multiome assay) were grouped into 17 pools, with 10 in each pool. The donors in each pool were both condition (control or AUD) and sex balanced. The nuclei isolation for each pool is similar to the procedure described for the aforementioned single cell multiome assay. Zero point two (or One fifth) unit per microliter of RNase inhibitor was used in the buffers.

10X HT Single-nuclei RNA-seq Library Preparation and Sequencing

The Chromium Next GEM single cell 3’ HT reagent kits v3.1 (user guide CG000416, 10X Genomics, Inc.) was used for the single-nuclei RNA-seq assay. The single nuclei suspension from a pool of 10 donor tissue samples were loaded into two wells of a Chromium Next GEM chip M to target 60,000 cell recovery per well. The chip was run on a Chromium X (10x Genomics). Single cell gel beads in emulsion containing barcoded oligonucleotides and reverse transcriptase reagents were generated. cDNA was synthesized and amplified following cell capture and cell lysis, The quality and

quantity of cDNA and resulting libraries were examined by Bioanalyzer. The final libraries were sequenced on an Illumina NovaSeq 6000. 100-bp reads including cell barcode and UMI sequences and 100-bp RNA reads were generated.

Cell ranger Count Analysis

Cell Ranger Count (cellranger-count-7.0.1, http://support.10xgenomics.com/) was utilized to process the raw sequence data derived from the single-cell multiome libraries. Both the ATAC and gene expression FASTQ files were processed with the cellranger-arc count algorithm. The reference refdata-cellranger-arc-GRCh38-2020-A-2.0.0 (10x Genomics) was used. The filtered gene-cell barcode matrices and fragment files were used for further analysis.

Demultiplexing

Cells from each of the 42 sequencing pools (25 from the single-cell multiome assay and 17 from the single-nuclei RNA-seq assay) were demultiplexed back into their samples of origin using the tool Demuxlet[69] with default parameters, which uses genotype variant information for each sample to predict the sample of origin for each cell barcode, as well as identify doublet cells, artifactual libraries generated when two cells are captured in the same droplet during library preparation. Between 55% and 75% of cells from each pool were identified as singlets and assigned to a sample. The remaining cells (identified as doublets or ambiguous) were removed from further analysis.

After demultiplexing, seven donors with less than 200 cell barcodes assigned were removed from all further analyses; all of the remaining 163 donors had over 1,000 barcodes. These 163 donors were used for all following analyses until the filtering step detailed in ‘Sample Filtering’, below.

Initial Quality Control

Unless specified differently, all following analysis was performed in R (version 4.3.1), predominantly utilizing the Seurat[70] (v5) and Signac[71] (v5) packages.

A Seurat object was created for each replicate from the HT assay using the gene expression count matrix from the Cell Ranger output (34 objects total). Cells with below 800 or above 11,250 genes, above 125,000 molecules, or above 10% mitochondrial RNA were removed from further analysis. These are commonly used quality control metrics to remove low-quality cells or multiplets. Each pool was then normalized using the scTransform() function in Seurat.

A Signac object, containing both RNA and ATAC-seq data, was created for each replicate from the multiome assay from the hdf5 file from the Cell Ranger output (50 objects total). Cells with below 800 or above 20,000 genes, below 800 or above

500,000 detected RNA molecules, or above 20% mitochondrial RNA were removed from further analysis. An additional round of filtering was performed using the ATAC-seq data. The following cells were removed from further analysis:

Cells with less than 100 or over 100,000 features;

Less than 100 or over 1,000,000 counts;

TSS enrichment less than 2;

Nucleosome signal greater than 4;

Percentage of reads in peaks less than 15%;

Total number of fragments in peaks less than 800 or over 100,000;

Ratio reads in genomic blacklist regions greater than 0.05

Between both assays, 1,307,323 cells passed all QC filters.

RNA-seq Integration and Visualization

After the above quality control, all cells from each of the 34 Seurat objects were integrated into the same Seurat object for visualization in the same 2D space. The atomic sketch integration method was used, a dictionary learning based procedure recently developed in Seurat for large datasets (see https://satijalab.org/seurat/articles/parsebio_sketch_integration). Briefly, 5,000 representative cells were selected from each pool (based on statistical leverage). Integration was performed on these sketched cells using the reference-based RPCAIntegration method. Then, each cell from each pool was placed in this integrated space as well using the ProjectIntegration function.

To visualize all cells in the same plot, we used functionality in the Seurat v5 and BPCells packages to convert each pool to an on-disk BPCells matrix.[72] This allowed us to merge each object in a memory-efficient way. After merging, the function RunUMAP was run on the combined object for 2D visualization.

Cell Type Annotation

The 1,307,323 cells were divided into 49 clusters using the FindNeighbors and FindClusters functions in Seurat. Cell clusters were annotated into known striatal cell types based on expression levels of a combination of marker genes curated from established studies (Figure 2B).[21,22,25,57,73]

ATAC-seq Integration and Visualization

Each of the 50 Signac objects were processed using the standard ATAC-seq procedure in Signac – FindTopFeatures, RunTFIDF, RunSVD – and all pools were then integrated using the IntegrateEmbeddings command.

UMAP visualization was calculated with the RunUMAP command, using the integrated_lsi reduction determined in the previous integration step. Cell type labels were transferred to ATAC-seq object using the assignments for each barcode determined from the RNA-seq data.

Sample Filtering

Following the above analyses, 20 samples with a proportion of glutamatergic neurons greater than 10% were removed, because such a cell-type composition indicates potential contamination with non-caudate tissue, leaving 143 samples for the following downstream analyses.

Cell Subtype/Substate Annotation and Testing

Microglia and astrocyte clusters were further divided into four and two subclusters, respectively, by performing another iteration of FindNeighbors and FindClusters on these individual clusters, using cells from the 143 samples (see above). Subcluster-specific genes were determined by using the "roc" test within the FindMarkers function in Seurat (see https://satijalab.org/seurat/reference/findmarkers). Top 50 genes (based on myAUC statistic) were used as input into g:Profiler for each subcluster to determine enriched biological pathways specific to that subcluster.

For testing for a difference in the proportion of cell states in individuals with AUD, the mean proportion of cells in each cluster were calculated for each sample, and an ANOVA was performed to determine if the mean proportion significantly changed in AUD samples as compared to controls. Age, sex, and ethnic origin were used as covariates. For this test, we removed samples with fewer than 50 cells of the cell type being tested, as these samples contain very few cells of each subcluster and thus their mean is more unreliable.

Differential Expression Analysis

RNA Pseudobulk Samples Creation

Due to the sparsity of single-cell data, differential expression methods designed to be run on the single-cell level often lack high statistical power. To account for this challenge, we utilized a pseudobulk approach. To create the pseudobulk data, for each cell type, the gene expression matrices of each cell of that cell type were combined (summed) by sample ID. Samples were removed on a cell type-specific basis if the

sample contained less than 50 cells of that cell type. See Supplementary Table 7 for a summary of the number of pseudobulk samples created for each cell type. Due to a low number of samples (less than 10 AUD and 10 control) meeting the >=50 cell criteria, differential gene expression analysis was not performed for cholinergic interneurons, vascular smooth muscle cells, CCK interneurons, and macrophages. These pseudobulk samples were used for the differential expression analysis, below.

Differential Gene Expression Analysis

Differential gene expression analysis between AUD and control samples was performed for each cell type, as well as the two subclusters of astrocytes and four subclusters of microglia, using DESeq2,[74] a statistical package designed for bulk RNA-seq data, with the default parameters. Briefly, the tool estimates the variance of gene expression and then fits a negative binomial distribution to each gene, which accounts for the over-dispersion of RNA sequencing data, which can result in more accurate p-values. Sex, age (as a continuous variable), and ethnic origin were included as covariates in the models. Genes with p values of less than 0.2 (corrected for multiple-hypothesis testing using the Benjamini-Hochberg method) were deemed significant.

Gene Set Enrichment Analysis

Gene set enrichment analysis was performed for each cell type that underwent differential expression analysis, using the fgsea R package,[75] which uses a preranked list of genes to determine gene sets that are enriched based on the gene rankings. In this case, the AUD vs Control log fold changes from the differential expression analysis were used as the ranks, and pathways from the Reactome database were used as gene sets. See Supplementary Table 9 for full fgsea results for each cell type. For visualization, the top 30 enriched pathways (based on smallest Benjamini-Hochberg-adjusted p values) in each cell type were selected and hierarchically clustered based on number of genes shared between the pathways. Clustered pathways were then manually labeled into 25 groups.

Creation of Cell Type-specific ATAC-seq Profiles

CoveragePlot function in Signac was used for visualization of ATAC-seq signal for marker genes.

Peak calling was performed separately for cells from each of the 16 cell types (excluding glutamatergic neurons) using the CallPeaks function in Signac with default parameters. The function uses MACS2[76] for peak calling.

Gene-level chromatin accessibility information calculated from GeneActivity function (with default parameters) in Signac, defined as total counts in gene body and promoter region.

For comparing similarity of peaks called between cell types, the Jaccard index was used, defined here as the number of peaks in one cell type overlapping a peak in the other cell type, divided by the union of the peaks in both cell types.

All cells from the integrated ATAC-seq object, from the 143 samples determined after the 'Sample Filtering' step, above, were used for the procedures in this section.

Differential Chromatin Accessibility Analysis

ATAC Pseudobulk Samples Creation

In the same way as the RNA-seq data, pseudobulk chromatin accessibility data was created for the ATAC-seq data: For each cell type, the ATAC-seq counts matrices of each cell of that cell type were combined (summed) by sample ID, for the 143 samples. Samples were removed on a cell type-specific basis if the sample contained less than 50 cells of that cell type. See Supplementary Table 12 for a summary of the number of pseudobulk samples created for each cell type. Due to a low number of samples meeting the >=50 cell criteria, differential accessibility analysis was not performed for cholinergic interneurons, vSMCs, CCK interneurons, macrophages, ependymal cells, LTS interneurons, or endothelial cells.

Differential Accessibility Analysis

Differential chromatin accessibility analysis between AUD and control samples was performed for each cell type using DESeq2 with the default parameters. Sex, age, and ethnic origin were included as covariates in the models. Genes with p values of less than 0.2 (corrected for multiple-hypothesis testing using the Benjamini-Hochberg method) were deemed significant. Regions residing in promoter regions of genes was determined using R package ChIPSeeker.[77] Namely, the function annotatePeak() was used, with parameters: TxDb = TxDb.Hsapiens.UCSC.hg38.knownGene, annoDb="org.Hs.eg.db", and tssRegion = c(-1000, 1000).

Comparison of Differentially Accessible Genes and Differentially Expressed Genes

To calculate the association between gene expression and chromatin accessibility differences for each gene, we assigned to each gene with at least 1 DAR in the promoter region the log2 fold change of the DAR with the highest ATAC signal, as well as the log2 fold change of the gene's expression.

For the GSEA analyses, the AUD vs Control log fold changes from the differential expression analysis were used as the ranks, and genes with at least 1 DAR in the promoter region were used as the gene sets, separated into genes with positive log2 fold changes, and those with negative log2 fold changes.

Identifying Genes Containing Significant GWAS Loci

The two GWAS studies (Saunders, et al.[3] and Zhou et al.[5]) utilized in this study defined a locus as the region including all variants in linkage disequilibrium of r2> 0.1. For the present study, all 1,307 loci associated with the drinks per week (DrnkWk) phenotype from Saunders et al. were selected. To identify genes overlapping with these regions, gene annotations from UCSC Genome Browser for the hg38 genome assembly (implemented in the TxDb.Hsapiens.UCSC.hg38.knownGene R package[78]) were used. This identified 3,406 genes. A comparable process was used to select genes overlapping loci from the Zhou et al. study. All 75 loci associated with the problematic alcohol use phenotype were selected, which overlapped with 750 known genes from the UCSC annotations.

Variant Calling

Integrated snATAC-seq data were split into single bam files for each of the 143 individuals using sinto (https://timoast.github.io/sinto/). Duplicated bam files for the same sample were merged together with samtools.[79] For variant calling, the Sentieon germline variant calling pipeline[80] was used, namely:

Removal of duplicate RNA molecules;

Recalibration of base quality score using GATK's Base Quality Score Recalibration;

Variant calling was performed for each sample using the Sentieon's Haplotyper algorithm;

Joint variant calling was performed using the DNAseq algorithm;

Variants were recalibrated using GATK's Variant Quality Score Recalibration[81] algorithm; variants not passing the recalibration test were filtered out for further analyses.

eQTL Analysis

Expression quantitative trait loci (eQTL) analysis was performed for all SNPs in each cell type within 100,000 bases of a differentially expressed gene overlapping a GWAS loci and within an ATAC-seq peak from that cell type. tensorQTL[82] was used to perform the analysis using the map_cis function with default parameters. Variants with minor allele frequency < 0.05 were excluded from the analysis.

Gene Regulatory Mechanisms Prediction

<u>chromVAR[83]</u>

Prediction of motif activities for each cell was performed using the RunChromVAR command in Signac. Briefly, chromVAR identifies motifs associated with variability in chromatin accessibility between cells[83]). Differential testing on the chromVAR z-score was performed using the FindMarkers function, setting mean.fxn=rowMeans and fc.name="avg_diff", so that the fold-change represents the average difference in z-score between the groups.

To make these differential activity motif results more robust, we utilized a pseudobulk approach: averaging per-cell motif scores for all cells within a sample of a given cell type, taking the log, and then using an ANOVA – with sex, age, and ethnic origin as covariates – to test for differences between AUD and control. All samples used for differential accessibility testing (see 'ATAC Pseudobulk Samples Creation') were used for this analysis.

Gene Regulatory Network Inference

To build the cell population gene regulatory network, we used LINGER, as described in Yuan & Duren, 2024.[27] We generated pseudobulk-level expression and chromatin accessibility data for each donor and each cell type. Here we used the union set of peaks (described above) for ATAC-seq data. as well as a covariate matrix, with sex, age, and ethnic origin as covariates to the model. All samples used for differential accessibility testing (see 'ATAC Pseudobulk Samples Creation') were used for this analysis.

Trans-regulatory module detection by matrix factorization

To detect key TF-TG subnetworks (modules) from the cell population TF–TG trans-regulation, we use non-negative matrix factorization (NMF). Before matrix factorization, We normalize the trans-regulatory potential matrix by standardizing each row (TF) and each column (TG) independently. The standardization each TF ensures that for each TF, the average regulatory potential across TGs becomes zero, and the variation in regulatory potential across genes has a standard deviation of one. The same normalization is applied to each TG so that the effect of the regulator side is also normalized. We take the average of these two standardized matrices and set the negative values to zeros and use it for downstream analysis. Next, we performed NMF on the preprocessed matrix to decompose it into two non-negative matrices, W and H, representing module membership of TGs and TFs, respectively. W is a m by k module weight matrix for TF, representing module weight of TF, where m is the number of TF. H is a k by n matrix, representing module weight for TGs, where n is the number of TG. To assign TF and TG into specific modules, we normalize the module weight matrix to equal sum for different modules. For each gene, we convert the normalized weight matrix into proportions by diving the sum of weights across modules. We sort genes based on their highest proportion across all modules to select the top 10% of genes and assign them to modules for which the gene has the largest score.

This procedure was applied to TF module W matrix and the TG module H matrix. Here, we identified 10 trans-regulatory modules.

To uncover AUD-associated regulatory programs in each cell type, we performed differential module expression analysis. We first pre-processed the pseudo-bulk gene expression count matrix by: (1) normalizing for cell depth, (2) log-transforming, and (3) z-scoring expression across all donors. We then estimated module activity in each donor as the mean expression of module genes. Using a two sample t-test, we identified differentially active modules between control and AUD samples.

Identification of cis and trans-driver TFs.

We identify cis and trans driver TFs underlying epigenetic and transcriptome change between control and AUD using a linear regression model, $Y = A\beta + \beta_0 + \varepsilon$. For transcriptome drivers, the regression model predicted the log transformation of the gene expression fold change between the control and AUD samples (Y) from cell type-specific TF-TG trans-regulation (A). For epigenetic drivers, the model predicted chromatin accessibility changes (Y) from the cell type-specific TF-RE cis-regulation (A). Significant TFs from each model indicated TFs driving differential expression and chromatin states between conditions through direct epigenetic or transcriptome regulation.

Cell-cell Communication Analysis

To analyze cell-cell communication differences in AUD individuals, we used MultiNicheNet,[36] an R package for differential cell-cell communication analysis using single-cell data with multi-sample, multi-condition designs. All samples used for differential expression testing (see 'RNA Pseudobulk Samples Creation') were used for this analysis. User-set parameters were set as the following:

MultiNicheNet's analysis uses a pseudobulk approach, and the minimum number of cells per cell type per sample was set to 10, the recommended default;

Sex, ethnic origin, and age were used as covariates in the design;

For a differentially expressed gene to be further considered when calculating ligand activity, we choose for a minimum logFC of 0.50, maximum adjusted p-value of 0.2, and minimum fraction of expression of 0.05;

For the NicheNet ligand-target inference, the top 250 predicted target genes were considered;

The weights of the prioritization of expression, differential expression and NicheNet activity information was set to the recommended defaults (see https://github.com/saeyslab/multinichenetr);

Sender cell types were defined as astrocytes, microglia, and oligodendrocytes;

Receiver cell types were defined as astrocytes, microglia, and oligodendrocytes; Visualization of top 5 ligand-receptor pairs in AUD individuals, based on scaled ligand activity score, was created using the make_circos_group_comparison function.

References

1 Organization, W. H. *Global Status Report on Alcohol and Health 2018*. (World Health Organization, 2018).

2 *Diagnostic and statistical manual of mental disorders : DSM-5™*. 5th edition. edn, (American Psychiatric Publishing, a division of American Psychiatric Association, 2013).

3 Saunders, G. R. B. *et al.* Genetic diversity fuels gene discovery for tobacco and alcohol use. *Nature* **612**, 720-724 (2022). https://doi.org/10.1038/s41586-022-05477-4

4 Clarke, T. K. *et al.* Genome-wide association study of alcohol consumption and genetic overlap with other health-related traits in UK Biobank (N=112 117). *Molecular Psychiatry* **22**, 1376-1384 (2017). https://doi.org/10.1038/mp.2017.153

5 Zhou, H. *et al.* Multi-ancestry study of the genetics of problematic alcohol use in over 1 million individuals. *Nature Medicine* **29**, 3184-3192 (2023). https://doi.org/10.1038/s41591-023-02653-5

6 Kranzler, H. R. *et al.* Genome-wide association study of alcohol consumption and use disorder in 274,424 individuals from multiple populations. *Nature Communications* **10**, 1499 (2019). https://doi.org/10.1038/s41467-019-09480-8

7 Walters, R. K. *et al.* Transancestral GWAS of alcohol dependence reveals common genetic underpinnings with psychiatric disorders. *Nature Neuroscience* **21**, 1656-1669 (2018). https://doi.org/10.1038/s41593-018-0275-1

8 Bell, R. L. *et al.* Gene expression changes in the nucleus accumbens of alcohol-preferring rats following chronic ethanol consumption. *Pharmacology Biochemistry and Behavior* **94**, 131-147 (2009). https://doi.org/https://doi.org/10.1016/j.pbb.2009.07.019

9 Zhou, Z., Yuan, Q., Mash, D. C. & Goldman, D. Substance-specific and shared transcription and epigenetic changes in the human hippocampus chronically exposed to cocaine and alcohol. *Proceedings of the National Academy of Sciences* **108**, 6626-6631 (2011). https://doi.org/10.1073/pnas.1018514108

10 Farris, S. P., Arasappan, D., Hunicke-Smith, S., Harris, R. A. & Mayfield, R. D. Transcriptome organization for chronic alcohol abuse in human brain. *Molecular Psychiatry* **20**, 1438-1447 (2015). https://doi.org/10.1038/mp.2014.159

11 Kapoor, M. *et al.* Multi-omics integration analysis identifies novel genes for alcoholism with potential overlap with neurodegenerative diseases. *Nature Communications* **12**, 5071 (2021). https://doi.org/10.1038/s41467-021-25392-y

12 McClintick, J. N., Thapa, K., Liu, Y., Xuei, X. & Edenberg, H. J. Effects of chronic intermittent ethanol exposure and withdrawal on neuroblastoma cell transcriptome. *Alcohol* **85**, 119-126 (2020). https://doi.org/10.1016/j.alcohol.2019.12.004

13 Brenner, E. *et al.* Single cell transcriptome profiling of the human alcohol-dependent brain. *Human Molecular Genetics* **29**, 1144-1153 (2020). https://doi.org/10.1093/hmg/ddaa038

14 Buenrostro, J. D., Wu, B., Chang, H. Y. & Greenleaf, W. J. ATAC-seq: A Method for Assaying Chromatin Accessibility Genome-Wide. *Current Protocols in Molecular Biology* **109**, 21.29.21-21.29.29 (2015). https://doi.org/https://doi.org/10.1002/0471142727.mb2129s109

15 Krishnan, H. R. *et al.* Unraveling the epigenomic and transcriptomic interplay during alcohol-induced anxiolysis. *Molecular Psychiatry* **27**, 4624-4632 (2022). https://doi.org/10.1038/s41380-022-01732-2
16 Koob, G. F. & Volkow, N. D. Neurocircuitry of Addiction. *Neuropsychopharmacology* **35**, 217-238 (2010). https://doi.org/10.1038/npp.2009.110
17 Garavan, H. *et al.* Cue-Induced Cocaine Craving: Neuroanatomical Specificity for Drug Users and Drug Stimuli. *American Journal of Psychiatry* **157**, 1789-1798 (2000). https://doi.org/10.1176/appi.ajp.157.11.1789
18 Liu, H.-S. *et al.* Dorsolateral caudate nucleus differentiates cocaine from natural reward-associated contextual cues. *Proceedings of the National Academy of Sciences* **110**, 4093-4098 (2013). https://doi.org/10.1073/pnas.1207531110
19 Lovinger, D. M. & Alvarez, V. A. Alcohol and basal ganglia circuitry: Animal models. *Neuropharmacology* **122**, 46-55 (2017). https://doi.org/10.1016/j.neuropharm.2017.03.023
20 Everitt, B. J. & Robbins, T. W. Neural systems of reinforcement for drug addiction: from actions to habits to compulsion. *Nat Neurosci* **8**, 1481-1489 (2005). https://doi.org/10.1038/nn1579
21 Grecco, G. G. *et al.* A multi-omic analysis of the dorsal striatum in an animal model of divergent genetic risk for alcohol use disorder. *J Neurochem* **157**, 1013-1031 (2021). https://doi.org/10.1111/jnc.15226
22 Tepper, J. M., Tecuapetla F Fau - Koós, T., Koós T Fau - Ibáñez-Sandoval, O. & Ibáñez-Sandoval, O. Heterogeneity and diversity of striatal GABAergic interneurons. *Front Neuroanat.* **4** (2010). https://doi.org/10.3389/fnana.2010.00150
23 Sinner, P. *et al.* Microglial expression of CD83 governs cellular activation and restrains neuroinflammation in experimental autoimmune encephalomyelitis. *Nature Communications* **14**, 4601 (2023). https://doi.org/10.1038/s41467-023-40370-2
24 Brimblecombe, K. R. & Cragg, S. J. The Striosome and Matrix Compartments of the Striatum: A Path through the Labyrinth from Neurochemistry toward Function. *ACS Chemical Neuroscience* **8**, 235-242 (2017). https://doi.org/10.1021/acschemneuro.6b00333
25 He, J. *et al.* Transcriptional and anatomical diversity of medium spiny neurons in the primate striatum. *Current Biology* **31**, 5473-5486.e5476 (2021). https://doi.org/https://doi.org/10.1016/j.cub.2021.10.015
26 Jassal, B. *et al.* The reactome pathway knowledgebase. *Nucleic Acids Research* **48**, D498-D503 (2020). https://doi.org/10.1093/nar/gkz1031
27 Yuan, Q. & Duren, Z. Inferring gene regulatory networks from single-cell multiome data using atlas-scale external data. *Nature Biotechnology* (2024). https://doi.org/10.1038/s41587-024-02182-7
28 Dong, D. *et al.* Inflammasome activity is controlled by ZBTB16-dependent SUMOylation of ASC. *Nature Communications* **14**, 8465 (2023). https://doi.org/10.1038/s41467-023-43945-1
29 Xu, H.-j. *et al.* Gibberellic acid targeting ZBTB16 reduces NF-κB dependent inflammatory stress in sepsis-induced neuroinflammation. *European Journal of*

Pharmacology **976**, 176665 (2024). https://doi.org/https://doi.org/10.1016/j.ejphar.2024.176665
30 Usui, N. *et al.* Zbtb16 regulates social cognitive behaviors and neocortical development. *Translational Psychiatry* **11**, 242 (2021). https://doi.org/10.1038/s41398-021-01358-y
31 Schumann, G. *et al.* KLB is associated with alcohol drinking, and its gene product β-Klotho is necessary for FGF21 regulation of alcohol preference. *Proceedings of the National Academy of Sciences* **113**, 14372-14377 (2016). https://doi.org/10.1073/pnas.1611243113
32 Langfelder, P. & Horvath, S. WGCNA: an R package for weighted correlation network analysis. *BMC Bioinformatics* **9**, 559 (2008). https://doi.org/10.1186/1471-2105-9-559
33 Schep, A. N., Wu, B., Buenrostro, J. D. & Greenleaf, W. J. chromVAR: inferring transcription-factor-associated accessibility from single-cell epigenomic data. *Nature Methods* **14**, 975-978 (2017). https://doi.org/10.1038/nmeth.4401
34 Vinson, C. *et al.* Classification of Human B-ZIP Proteins Based on Dimerization Properties. *Molecular and Cellular Biology* **22**, 6321-6335 (2002). https://doi.org/10.1128/MCB.22.18.6321-6335.2002
35 Liddelow, S. A. *et al.* Neurotoxic reactive astrocytes are induced by activated microglia. *Nature* **541**, 481-487 (2017). https://doi.org/10.1038/nature21029
36 Browaeys, R. *et al.* MultiNicheNet: a flexible framework for differential cell-cell communication analysis from multi-sample multi-condition single-cell transcriptomics data. *bioRxiv*, 2023.2006.2013.544751 (2023). https://doi.org/10.1101/2023.06.13.544751
37 Repovic, P., Mi, K. & Benveniste, E. N. Oncostatin M enhances the expression of prostaglandin E2 and cyclooxygenase-2 in astrocytes: synergy with interleukin-1beta, tumor necrosis factor-alpha, and bacterial lipopolysaccharide. *Glia* **42**, 433-446 (2003). https://doi.org/10.1002/glia.10182
38 Siletti, K. *et al.* Transcriptomic diversity of cell types across the adult human brain. *Science* **382**, eadd7046 (2023). https://doi.org/10.1126/science.add7046
39 Zhang, D. *et al.* Synaptic-like transmission between neural axons and arteriolar smooth muscle cells drives cerebral neurovascular coupling. *Nature Neuroscience* **27**, 232-248 (2024). https://doi.org/10.1038/s41593-023-01515-0
40 Balogh, E. *et al.* Effects of acute alcohol consumption on neuronal activity and cerebral vasomotor response. *Neurol Sci* **43**, 625-631 (2022). https://doi.org/10.1007/s10072-021-05273-4
41 Crews, F. T. *et al.* Neuroimmune Function and the Consequences of Alcohol Exposure. *Alcohol Res* **37**, 331-341, 344-351 (2015).
42 Lowe, P. P. *et al.* Chronic alcohol-induced neuroinflammation involves CCR2/5-dependent peripheral macrophage infiltration and microglia alterations. *J Neuroinflammation* **17**, 296 (2020). https://doi.org/10.1186/s12974-020-01972-5
43 Kamal, H. *et al.* Alcohol Use Disorder, Neurodegeneration, Alzheimer's and Parkinson's Disease: Interplay Between Oxidative Stress, Neuroimmune Response and Excitotoxicity. *Front Cell Neurosci.* **14**, 282 (2020).

44 Adermark, L. & Bowers, M. S. Disentangling the Role of Astrocytes in Alcohol Use Disorder. *Alcohol Clin Exp Res* **40**, 1802-1816 (2016). https://doi.org/10.1111/acer.13168
45 Gawliński, D., Gawlińska, K., Frankowska, M. & Filip, M. Cocaine and Its Abstinence Condition Modulate Striatal and Hippocampal Wnt Signaling in a Male Rat Model of Drug Self-Administration. *International Journal of Molecular Sciences* **23** (2022).
46 Fields, R. D. Oligodendrocytes changing the rules: action potentials in glia and oligodendrocytes controlling action potentials. *Neuroscientist* **14**, 540-543 (2008). https://doi.org/10.1177/1073858408320294
47 Káradóttir, R. & Attwell, D. Neurotransmitter receptors in the life and death of oligodendrocytes. *Neuroscience* **145**, 1426-1438 (2007). https://doi.org/https://doi.org/10.1016/j.neuroscience.2006.08.070
48 Buffo, A. *et al.* Expression pattern of the transcription factor Olig2 in response to brain injuries: Implications for neuronal repair. *Proceedings of the National Academy of Sciences* **102**, 18183-18188 (2005). https://doi.org/10.1073/pnas.0506535102
49 Zhang, K. *et al.* The Oligodendrocyte Transcription Factor 2 OLIG2 regulates transcriptional repression during myelinogenesis in rodents. *Nature Communications* **13**, 1423 (2022). https://doi.org/10.1038/s41467-022-29068-z
50 Mei, F. *et al.* Stage-Specific Deletion of Olig2 Conveys Opposing Functions on Differentiation and Maturation of Oligodendrocytes. *The Journal of Neuroscience* **33**, 8454 (2013). https://doi.org/10.1523/JNEUROSCI.2453-12.2013
51 Chao, C. C., Hu, S. X., Ehrlich, L. & Peterson, P. K. Interleukin-1 and Tumor Necrosis Factor-α Synergistically Mediate Neurotoxicity: Involvement of Nitric Oxide and of N-Methyl-D-aspartate Receptors. *Brain, Behavior, and Immunity* **9**, 355-365 (1995). https://doi.org/https://doi.org/10.1006/brbi.1995.1033
52 Chen, C. P., Kuhn, P., Chaturvedi, K., Boyadjieva, N. & Sarkar, D. K. Ethanol Induces Apoptotic Death of Developing β-Endorphin Neurons via Suppression of Cyclic Adenosine Monophosphate Production and Activation of Transforming Growth Factor-β1-Linked Apoptotic Signaling. *Molecular Pharmacology* **69**, 706 (2006). https://doi.org/10.1124/mol.105.017004
53 Kuhn, P. & Sarkar, D. K. Ethanol Induces Apoptotic Death of β-Endorphin Neurons in the Rat Hypothalamus by a TGF-β1-Dependent Mechanism. *Alcoholism: Clinical and Experimental Research* **32**, 706-714 (2008). https://doi.org/https://doi.org/10.1111/j.1530-0277.2008.00627.x
54 Flanders, K. C., Ren, R. F. & Lippa, C. F. TRANSFORMING GROWTH FACTOR-βS IN NEURODEGENERATIVE DISEASE. *Progress in Neurobiology* **54**, 71-85 (1998). https://doi.org/https://doi.org/10.1016/S0301-0082(97)00066-X
55 Hamaguchi, M. *et al.* Circulating transforming growth factor-β1 facilitates remyelination in the adult central nervous system. *eLife* **8**, e41869 (2019). https://doi.org/10.7554/eLife.41869
56 Ferguson, L. B. *et al.* Dissecting Brain Networks Underlying Alcohol Binge Drinking Using a Systems Genomics Approach. *Mol Neurobiol* **56**, 2791-2810 (2019). https://doi.org/10.1007/s12035-018-1252-0

57 Saunders, A. *et al.* Molecular Diversity and Specializations among the Cells of the Adult Mouse Brain. *Cell* **174**, 1015-1030 (2018). https://doi.org/10.1016/j.cell.2018.07.028
58 Gagnon, D. *et al.* Striatal Neurons Expressing D(1) and D(2) Receptors are Morphologically Distinct and Differently Affected by Dopamine Denervation in Mice. *Sci Rep* **7**, 41432 (2017). https://doi.org/10.1038/srep41432
59 Phan, B. N. *et al.* Single nuclei transcriptomics in human and non-human primate striatum in opioid use disorder. *Nature Communications* **15**, 878 (2024). https://doi.org/10.1038/s41467-024-45165-7
60 McClintick, J. N. *et al.* Gene expression changes in the ventral hippocampus and medial prefrontal cortex of adolescent alcohol-preferring (P) rats following binge-like alcohol drinking. *Alcohol* **68**, 37-47 (2018). https://doi.org/10.1016/j.alcohol.2017.09.002
61 Lesscher, H. M. B., Bailey, A. & Vanderschuren, L. Genetic Variability in Adenosine Deaminase-Like Contributes to Variation in Alcohol Preference in Mice. *Alcohol Clin Exp Res* **41**, 1271-1279 (2017). https://doi.org/10.1111/acer.13409
62 Thompson, S. L. *et al.* Btbd3 expression regulates compulsive-like and exploratory behaviors in mice. *Translational Psychiatry* **9**, 222 (2019). https://doi.org/10.1038/s41398-019-0558-7
63 Garnett, C., Kastaun, S., Brown, J. & Kotz, D. Alcohol consumption and associations with sociodemographic and health-related characteristics in Germany: A population survey. *Addict Behav* **125**, 107159 (2022). https://doi.org/10.1016/j.addbeh.2021.107159
64 Benjamin, K. J. M. *et al.* Analysis of gene expression in the postmortem brain of neurotypical Black Americans reveals contributions of genetic ancestry. *Nature Neuroscience* **27**, 1064-1074 (2024). https://doi.org/10.1038/s41593-024-01636-0
65 Sutherland, G. T. *et al.* The NSW brain tissue resource centre: Banking for alcohol and major neuropsychiatric disorders research. *Alcohol* **52**, 33-39 (2016). https://doi.org/https://doi.org/10.1016/j.alcohol.2016.02.005
66 Das, S. *et al.* Next-generation genotype imputation service and methods. *Nature Genetics* **48**, 1284-1287 (2016). https://doi.org/10.1038/ng.3656
67 Loh, P.-R., Palamara, P. F. & Price, A. L. Fast and accurate long-range phasing in a UK Biobank cohort. *Nature Genetics* **48**, 811-816 (2016). https://doi.org/10.1038/ng.3571
68 Taliun, D. *et al.* Sequencing of 53,831 diverse genomes from the NHLBI TOPMed Program. *Nature* **590**, 290-299 (2021). https://doi.org/10.1038/s41586-021-03205-y
69 Kang, H. M. *et al.* Multiplexed droplet single-cell RNA-sequencing using natural genetic variation. *Nature Biotechnology* **36**, 89-94 (2018). https://doi.org/10.1038/nbt.4042
70 Hao, Y. *et al.* Dictionary learning for integrative, multimodal and scalable single-cell analysis. *Nature Biotechnology* **42**, 293-304 (2024). https://doi.org/10.1038/s41587-023-01767-y

71 Stuart, T., Srivastava, A., Madad, S., Lareau, C. A. & Satija, R. Single-cell chromatin state analysis with Signac. *Nature Methods* **18**, 1333-1341 (2021). https://doi.org/10.1038/s41592-021-01282-5
72 Parks, B. (https://bnprks.github.io/BPCells, 2024).
73 Zillich, L. *et al.* Multi-omics signatures of alcohol use disorder in the dorsal and ventral striatum. *Transl Psychiatry* **12**, 190 (2022). https://doi.org/10.1038/s41398-022-01959-1
74 Love, M. I., Huber, W. & Anders, S. Moderated estimation of fold change and dispersion for RNA-seq data with DESeq2. *Genome Biology* **15**, 550 (2014). https://doi.org/10.1186/s13059-014-0550-8
75 Korotkevich, G. *et al.* Fast gene set enrichment analysis. *bioRxiv*, 060012 (2021). https://doi.org/10.1101/060012
76 Zhang, Y. *et al.* Model-based Analysis of ChIP-Seq (MACS). *Genome Biology* **9**, R137 (2008). https://doi.org/10.1186/gb-2008-9-9-r137
77 Yu, G., Wang, L.-G. & He, Q.-Y. ChIPseeker: an R/Bioconductor package for ChIP peak annotation, comparison and visualization. *Bioinformatics* **31**, 2382-2383 (2015). https://doi.org/10.1093/bioinformatics/btv145
78 Team, B. & Maintainer, B. TxDb.Hsapiens.UCSC.hg38.knownGene: Annotation package for TxDb object(s). . *R package version 3.4.6.* (2019).
79 Danecek, P. *et al.* Twelve years of SAMtools and BCFtools. *GigaScience* **10**, giab008 (2021). https://doi.org/10.1093/gigascience/giab008
80 Weber, J. A., Aldana, R., Gallagher, B. D. & Edwards, J. S. Sentieon DNA pipeline for variant detection - Software-only solution, over 20× faster than GATK 3.3 with identical results. *PeerJ PrePrints* **4**, e1672v1672 (2016). https://doi.org/10.7287/peerj.preprints.1672v2
81 van der Auwera, G. & O'Connor, B. D. *Genomics in the Cloud: Using Docker, GATK, and WDL in Terra*. (O'Reilly Media, Incorporated, 2020).
82 Taylor-Weiner, A. *et al.* Scaling computational genomics to millions of individuals with GPUs. *Genome Biology* **20**, 228 (2019). https://doi.org/10.1186/s13059-019-1836-7
83 Molina-Gonzalez, I., Miron, V. E. & Antel, J. P. Chronic oligodendrocyte injury in central nervous system pathologies. *Communications Biology* **5**, 1274 (2022). https://doi.org/10.1038/s42003-022-04248-1